Atomically precise control in the design of low-nuclearity supported metal catalysts

Originally published in:
Nature Reviews Materials 6(11), https://doi.org/10.1038/s41578-021-00360-6

Atomically-precise control in the design of low-nuclearity supported metal catalysts

Sharon Mitchell, Javier Pérez-Ramírez

Institute for Chemical and Bioengineering, Department of Chemistry and Applied Biosciences, ETH Zurich, Vladimir-Prelog-Weg 1, 8093 Zurich, Switzerland.
Corresponding author e-mail: jpr@chem.ethz.ch

Cite this article: S. Mitchell, J. Pérez-Ramírez. Atomically precise control in the design of low-nuclearity supported metal catalysts. *Nat. Rev. Mater.* **2021**, *6*, 969-985 (doi:10.1038/s41578-021-00360-6).

Abstract

Nanostructured catalysts incorporating supported metal atoms or small clusters of defined size and chemical composition attract considerable attention because of their potential to maximize resource efficiency. When optimally assembled, all the metal nuclei can participate in the catalytic cycle with properties tailored to deliver high specific activity and stable performance. Over the past decade, both the number and diversity of reported systems have exploded as researchers attempt to control the nanostructure with increasing atomic precision. Nonetheless, spatially resolving the architecture and properties of supported low-nuclearity catalysts remains challenging using existing analytical methods. After identifying general structural features of this advanced family of catalytic materials, including the composition, nuclearity, coordination environment, and location, as well as dynamic effects in reactive environments, our contribution critically examines progress in their control and understanding. State-of-the-art experimental and theoretical approaches for the characterization are explored, addressing strengths and limitations through recent case studies. Finally, we outline directions for future work that will cross frontiers in the design of catalytic materials, which will be indispensable for developing high-performing new architectures for sustainable technologies.

Introduction

The potential of catalytic solids to maximize the atom economy, increase energy efficiency, and reduce waste in chemical transformations makes them a central pillar for developing sustainable technologies to accelerate the transition to carbon-neutral chemical value chains using renewable feedstocks. During the last decades, guided by advances in synthetic and analytical methods, efforts to improve their effectiveness have increasingly focused on tailoring the nanostructure with atomic-level precision, leading to several breakthroughs in performance[1-4].

Catalytic materials integrating metal entities of defined nuclearity and composition are widely studied due to their extensive use in the chemical industry[5-7]. Low-nuclearity species, ranging from single-atom heterogeneous catalysts[8,9] to supported clusters of at most a few tens of atoms, draw attention for two main reasons. Depending on the architecture, all the metal nuclei can potentially participate in the catalytic cycle. Besides they can originate specific, in some cases unprecedented, reactivity[10,11]. These features are attractive for both the effective utilization of catalysts based on scarce precious metals and paving the way for the more widespread application of earth-abundant base metals in future catalytic processes.

Changing the nuclearity can significantly alter the geometric and electronic properties and associated reactivity of metal species, and the choice needs careful consideration. When supported on common carriers, including carbon-based materials and metal oxides, single atoms are often oxidic in character, which can alter the adsorption energy of intermediates compared to metal nanoparticles. They also lack neighbouring metal atoms, preventing them from catalysing reaction paths requiring larger atomic ensembles. Depending on the molecular-level requirements of the targeted application, these characteristics may benefit or limit their performance[10]. On the other hand, the properties of small metal clusters vary non-linearly depending on the specific interaction with carriers and the effects of electron confinement, and in many cases the atom-by-atom behaviour is still not fully understood[6].

Accordingly, the development of high-performance catalysts based on supported metal atoms or clusters requires an ability to precisely control the assembly and structure of active sites and relate this to their associated reactivity patterns. Success relies on the availability of techniques that can discriminate several fundamental properties. However, the spatial resolution of these tiny species at the atomic scale still poses an incredible challenge. The fact that practically relevant host materials typically have irregular three-dimensional morphologies and exhibit non-uniform surface structures and compositions compounds the difficulty because of the high resulting polydispersity of coordination sites. There is also growing awareness that small metal entities often contain chemically distinct atoms, for example, *p*-block elements or halogens. These atoms may come from the carrier or the chemisorption of simple ligands and determine their stability and associated properties. For this reason, most fundamental insights about the effects of nuclearity on structure-performance relationships derive from the study of simplified systems such as clusters in the gas phase[12] or anchored on single-crystal surfaces[6]. Besides, under reaction conditions, for example at elevated temperature, pressure, potential, and in the presence of distinct chemical species, various structural isomers of low-nuclearity species may coexist and interconvert from one to another, a phenomenon referred to as fluxionality[13].

The potential for emerging low-nuclearity catalysts to surpass the performance of conventionally supported metal nanoparticles together with the additional complexity for their structure elucidation calls for a critical analysis of our understanding of their controlled assembly and properties. In this review, we explore key characteristics in the design of catalytic solids integrating well-defined low-nuclearity metal species, concentrating on sizes of less than ten atoms (**Fig. 1**). After introducing the principal synthetic approaches for their stabilization, we examine the scope of characterization tools for discriminating the nuclearity, composition, geometry, and local environment of metal ensembles of distinct size, comparing experimental and theoretical insights. We also survey evidence of structural dynamics and

evolution from operando studies under reaction conditions, discussing relevant timescales and the implications for establishing structure-function relationships using knowledge from the analytical methods described. Finally, we set out future research directions that will guide their design and improve their innovation prospects.

Synthesis of low-nuclearity catalysts

Subnanometre-sized metal species dispersed on solid supports are pervasive in industrial catalysts. In this size range, the total number of atoms converges with the number of surface atoms, permitting a high utilisation of active phases, especially relevant for those containing scarce elements. Except for single-atom heterogeneous catalysts, where extensive synthetic efforts have targeted broadening the system diversity and tailoring the properties[8,9], methods to prepare low-nuclearity catalysts with atomic control are limited[14]. Here, we briefly recap reported strategies to stabilize metal species of defined nuclearity, discussing their versatility.

Deposition of defined precursors

Some of the first relationships between the nanostructures of low-nuclearity species and reactivity patterns came from studies of mass-selected clusters in the gas phase[12,15]. By avoiding the enormous complexity of applied catalytic materials, gas-phase experiments comprise a valuable approach to investigate the energetics and kinetics of elementary steps in catalysed reactions over atoms or clusters of defined size and composition[12]. However, since most studies address chemical transformations over charged coordinatively unsaturated species in the absence of interactions with ligands and supports, translating this knowledge to realistic systems remains complex.

In this direction, combining mass selection with cluster landing, typically under ‘soft’ conditions to preserve the cluster and substrate integrity, permits the obtainment of supported analogues with broad control over size, coverage, and composition (**Fig. 2a**). Mass-selected soft-landing approaches have provided unparalleled atomically-resolved insights into the

property and reactivity trends of low-nuclearity clusters[6,16]. However, the technique has several well-known limitations. Although deposition is possible on various carriers, they generally comprise (semi-)conductive low-index single crystal surfaces to minimise substrate charging and ensure the stabilization of well-defined clusters. Usually, the deposition and subsequent analysis are conducted under ultra-high vacuum conditions, far from practically-relevant processes. Advances towards the ambient ion soft landing through electrospray ionization show one direction to overcome these constraints, but the control over cluster size and arrangement remains limited. A general finding of cluster deposition approaches is that size effects depend strongly upon the specific modes of interaction with supports or reaction conditions and the associated impact on the structure or stoichiometry[16].

Bridging the gap between ultra-high vacuum studies and applied catalytic processes requires operating at higher pressures, temperatures, or potentials, with more complex reaction feeds and technologically-relevant materials. However, the stabilization of precisely-defined low-nuclearity clusters on porous and irregular supports continues to be challenging. Moreover, studies of metal species supported by mass-selected landing often only tested catalysts for short times, without monitoring the evolution of cluster sizes on structures[6], providing few insights on their stability. Typically, systems prepared by mass-selected landing contain low metal loadings (0.1 wt%) to prevent aggregation, which poses another challenge for their accurate characterization.

An alternative approach to size selection is to exploit the robust cluster frames of molecular complexes of defined metal nuclearity, permitting their deposition onto carriers by wet-chemical routes, typically followed by a thermal activation step to remove remaining ligands. Early studies demonstrated the preserved structural integrity of supported Ir_4 and Ir_6 species derived from their corresponding carbonyl salts[17]. Now widely studied, this strategy is amenable to various combinations of metals and support materials and offers broad scope in achievable nuclearity.[18-22] For example, the wet deposition of platinum tiara complexes

permitted the stabilization of clusters of sizes between 5-13 atoms carbons (**Fig. 2b**)[19]. However, the approach requires the availability of precursors that preserve their core structure in solution, upon interaction with the support, and in successive post-treatments to tailor the properties, which requires careful choice of ligands and conditions. Additional measures can improve the success, such as choosing a host material that integrates coordination sites that can anchor the desired species (for example, by confinement or ensuring a strong interaction)[20,22] or the creation of pinning points (for example, by creating a specific overlayer before the deposition)[23]. Wet-chemical approaches are considered broadly suitable for scalable production. Nonetheless, attention to the costs and potential hazards associated with the ligands and solvents applied is essential.

Sequential self-limiting growth

Another strategy to deposit well-defined clusters in gas-phase syntheses besides mass selection is surface reaction control, which is the underlying principle of atomic layer deposition (ALD)[24]. The self-limiting nature of ALD permits high coverages over complex three-dimensional support surfaces typical of nanoporous catalysts in a more scalable manner. While ALD initially attracted interest for the deposition of thin films in layer-by-layer treatments, nucleation-based growth modes permit the preparation of discrete nanoparticles with controllable properties. Adjusting the number of ALD cycles[25] and the density of anchoring sites[26,27] extended the technique scope to the fabrication of single atoms. To date, examples of single-atom catalysts (SACs) prepared by ALD are mainly limited to carbons such as graphene, likely because of the ease of creating isolated and abundant reactive surface groups in these materials through the introduction of heteroatoms or defects[28].

Compared to single atoms, the use of ALD for the controlled preparation of other low-nuclearity clusters remains limited to a handful of examples. By using isolated Pt atoms as nucleation sites for a second ALD cycle, both homonuclear (Pt_2)[29] and heteronuclear (Ru-Pt)[30] dimers have also been obtained (**Fig. 2b**). The distinct interaction of the metal precursor with

the pre-supported metal atoms and the carrier in the second step permitted the preferential formation of dimeric species. In both cases, the requirement for costly precursors containing bulky ligands such as methylcyclopentadienyl to ensure site isolation through steric interactions is unsuitable for practical applications. Few examples exist of the bottom-up synthesis of higher-nuclearity clusters. In the metal-organic framework (MOF) NU-1000, the specific structure of metal nodes and the corresponding arrangement of reactive hydroxyl groups within the pore structure enabled the fabrication of nickel tetrameric clusters[31].

Confinement or specific interactions

Several other methods have been reported for the synthesis of atomically-dispersed uniform clusters, often lacking a complete mechanistic understanding of the preferential formation of the observed species. Both homonuclear[32,33] and heteronuclear[34] entities of distinct size were obtained via pyrolysis routes, which have been widely applied in the synthesis of SACs. Most approaches target the uniform distribution of metal precursors, which may also be size selected, into porous carbon-based materials before carbonization, either by introducing them during the synthesis of a polymer precursor[34] or adsorbing them into crystallographically-defined positions within MOFs[32,33]. However, even if initially well dispersed in the carbon precursor, controlling the specific interaction of metal species with the carrier is expected to be critical to obtaining the desired size[35]. For example, confinement within pore networks and strong binding to heteroatoms in organic precursors can introduce physical barriers that reduce the propensity for diffusion, aggregation, or dispersion of metal species[36]. Recent work highlighted the potential for modulating the nuclearity of bimetallic systems by varying the metal identity and stoichiometry (**Fig. 2d**)[33], which presumably also derives from differences in specific interaction.

In wet-chemical syntheses, interactions between metal precursors can be exploited to construct well-defined reaction surface sites. An early example was the dimerization of vanadium complexes on a silica carrier[37]. Specific metal nuclearities may be energetically

favourable even in the absence of directing ligands. For instance, platinum dimers with atom-atom spacings of approximately 0.25 nm formed following the wet deposition of platinum nitrate onto graphitic carbon nitride (**Fig. 2e**), consistent with the favourable energy profiles for the association of pairs of metal atoms from neighbouring positions evidenced by density functional theory (DFT) and kinetic Monte Carlo (kMC) simulations, respectively[38]. In separate work, heteronuclear Pt-Ru dimers were stabilized in the intrinsic cavities of graphitic carbon nitride by a one-pot ice-assisted photocatalytic reduction method[39]. Platinum trimers were also identified to be the stable species on a Co-Pd core-shell nanocatalyst[40]. Other approaches have also exploited a bonding affinity either with an isolated metal in the host[41] or between two metals introduced simultaneously[42] to deposit heteronuclear dimers (**Fig. 2f**). Confinement effects in porous materials coupled with control of the metal loading can also direct preferential speciation. For example, the ion exchange and subsequent reduction of silver nitrate in Na-A zeolite led to the predominant formation of Ag_6 clusters[43]. Pd_4 clusters were also isolated in MOFs via ion exchange, taking advantage of the specific crystallographic structure[44]. In conclusion, preliminary observations show that the controllability of approaches exploiting specific interactions or confinement is highly system dependent. The preferences to form metal species of different nuclearity as a function of the carrier and synthetic conditions require deeper understanding through systematic experimental and theoretical assessment.

Size and composition of metal species

The ability to resolve the number and type of atoms in the smallest metal species is core to the design of low-nuclearity clusters, as each one can influence the structure and properties significantly. Though not without limitations, the direct visualization of the atomic structure undoubtedly comprises the most readily interpretable approach to access the nuclearity[21,40,45]. Now widely accessible, aberration-corrected scanning transmission electron microscopy

(AC-STEM) in annular dark field modes readily distinguishes contrast between low-nuclearity species on supports that have a sufficiently distinct (typically lighter) atomic number. The first reports of the visualization of single atoms in catalytic materials[46,47] paved the way for rapid growth in the topic of single-atom heterogeneous catalysts. Elegant examples of the imaging of other low-nuclearity species also exist.

Even in catalytic materials integrating well-defined metal clusters with strong phase contrast, precise discrimination of the number of atoms may be challenging without careful analysis of intensity profiles (**Fig. 3a**) coupled with tilting experiments to confirm the location[21]. When analysing supports with more irregular structures, multiple orientations of low-nuclearity species, sometimes dynamically interconnected, can further hamper the determination of metal ensemble size by simple visual inspection. One approach that can help to discriminate the size is the statistical nearest-neighbour analysis. Comparison of palladium species, derived from precursors of distinct nuclearity on graphitic carbon nitride, identified a good agreement between the measured nearest-neighbour distance distributions and the theoretical distribution for a random dispersion of atoms in the case of the mononuclear precursor. In contrast, appreciable shortening of the nearest neighbour distances was evident for palladium species derived from trimeric complexes (**Fig. 3b**)[22]. In the latter sample, the measured Pd-Pd distributions closely matched those estimated from the structures derived by molecular dynamics simulations. Nonetheless, this approach still relies on manual inspection of the multiple images to ensure that the observations are representative and assumes that the catalyst does not alter under the electron beam. In catalysts with high areal densities of metal species, overlapping ensembles can also complicate the analysis, affecting the measured distributions.

Regarding the composition, analysis of interatomic distances has shown that monometallic species may incorporate non-metal atoms. For example, iridium dimers were identified to exist as Ir-O-Ir structures with no direct metal-metal bond[21]. The separation of metal centres

by an oxygen atom breaks the metal ensemble, with clear implications for the catalytic performance since each iridium may behave like a single atom. The presence of non-metals in low-nuclearity metal clusters is not considered in the classical definition and raises the question of how such species should be classified. In this review, we regard any system that incorporates supported metal entities with a precise number of metal atoms of a given type to have that nuclearity.

To extend to bi- or multimetallic catalysts, it is also critical to discriminate the chemical identity of distinct metals. Using AC-STEM imaging approaches requires sufficient distinction in phase-contrast both between the metals and the carrier and between the different nuclei in the metal species. However, few visualization studies have distinguished between metal centres in heteronuclear supported atomic clusters, the composition of which is typically supported by insights derived from other techniques such as extended X-ray absorption fine structure (EXAFS)[42,48]. Exciting developments have demonstrated the potential of electron tomography for unravelling the composition and 3D arrangement of atoms in small metal clusters based on phase contrast. In the analysis of supported iron-platinum bimetallic nanoparticles, determination of the coordinates of all metal atoms (**Fig. 3c**)[49] provided new insights into chemical ordering at the single-atom level, while following the crystal nucleation in four dimensions[50], captured the structure and dynamics of the nanoparticle at early stages of growth. Coupled to TEM studies, electron energy loss spectroscopy (EELS) can verify the chemical identity of constituent elements with atomic resolution[51]. A particular advantage of EELS is the ability to detect single atoms of light elements, which are difficult to detect by TEM due to the smaller scattering powers, producing weak contrast, and higher knock-on probability, resulting in atom kick out during imaging. By isolation in carbon cages, EELS mapping of Li, F, Na, and Cl species permitted near-atomic precision (**Fig. 3d**)[52]. EELS also offers a path to detect the presence of transition

metal atoms on carriers of similar or higher relative mass as reported for Pt on CeO_2[53] or Ni on α-MoC[54].

Atom probe tomography (APT), which uses a field emission approach to analyse sample composition atomic layer by atomic layer, can provide complementary insights into nuclearity in materials that are challenging to study by AC-STEM, such as metal-host combinations with similar phase contrast. Since it requires some electrical conductivity, the technique is most well-suited for the characterization of metal alloys, but its application to semiconductors or ceramic materials by specialised methods for specimen preparation and analysis. The atomic-scale resolution of aluminium centres in zeolite catalysts provided information about the spatial distribution inaccessible by other analytical methods[55]. APT also identified copper and iron clusters of distinct size in metal-exchanged SSZ-13 zeolites used for the selective catalytic reduction of nitrous oxides[56,57]. Moving to other materials, the analysis of atomically-dispersed nickel sites in graphene evidenced the exclusive presence of isolated atoms located in vacancies in the host and coordinated to at least one nitrogen atom[58]. Although APT has the scope to accurately distinguish nuclearity and composition, the detailed assessment of these properties in low-nuclearity catalysts remains scarce. APT still has several limitations. As with AC-TEM, the small volumes sampled may not be representative of the entire sample. Besides, overlapping peaks in the experimental data from other ions can complicate the data interpretation[56]. A recent study also highlighted the insufficient understanding of imaging porous materials, showing that voids can lead to either an increase or a decrease in local atomic densities in the APT reconstruction[59].

Various other techniques, centred around characterizing atomic distances and bonding, can also shed light on whether single atoms or clusters are present in catalytic materials. Before advances in microscopy permitted their direct visualization, X-ray absorption spectroscopy (XAS) provided the main structural foundation for the description of cluster catalysis[7]. Derivation of the first shell coordination numbers of metal species coupled with an absence of

higher shell metal-metal bonding in iridium clusters derived from robust carbonyl complexes evidenced a good agreement with the structures expected based on X-ray crystallography of the metal precursors. However, the structures of supported clusters are often less well defined, and small departures in models lead to increased uncertainty in estimating cluster sizes based on nearest-neighbour analyses. In SACs, the absence of metal-metal bonds is widely regarded to support the sole presence of isolated atoms[9]. Nonetheless, a recent DFT and molecular dynamics analysis of Pd_x species on carbon nitride showed that variations in Pd-Pd bond lengths strongly affect metal-metal peaks in radial distribution functions, rendering their detection by EXAFS impossible[22]. These findings emphasize the importance of combining advanced modelling and simulation methods with other state-of-the-art experimental methods when interpreting EXAFS data. Another technique applied to confirm the spatial isolation of metal atoms is the infrared study of CO adsorption[60,61]. The sensitivity arises due to the variation in the stretching frequency of the CO adsorption band, which typically shifts to higher values when CO is bound to single atoms compared to larger metal ensembles. The technique scope is limited to certain types of catalytic materials, mainly platinum-based alloys. Previous studies showed that the electronic structure of host materials may prevent CO adsorption on isolated metal atoms[22], and a precise understanding of the relationship with cluster size is lacking[62].

Local atomic environment

Beyond size and composition, knowledge of local structure is imperative to understand reactivity patterns of low-nuclearity species. Important questions include the geometry that supported species adopt, how they coordinate to the host material, the chemical identity and arrangement of atoms around the adsorption site, and whether any ligands adsorb.

With crystalline supports, it is sometimes possible to directly visualize at least part of the local atomic environment. Elegant examples exist for single atoms on.graphene[63-65], metal

oxides[66] and sulfides[67], and metals[68]. Comparatively, reports of the local environments of other low-nuclearity structures in catalytic materials are scarce. Scanning tunnelling microscopy (STM) can potentially resolve the nanostructure of small clusters on model surfaces with atomic resolution but has rarely been applied with this precision with studies mainly focusing on cluster geometry[69-70]. The investigation of size-selected Pt_n clusters on TiO_2 showed that those smaller than seven atoms lay flat on the surface, while larger species underwent a planar to 3D transition[70]. These results highlighted the potential interplay between the strength of metal-metal bonding and interactions with the support. A key challenge is to overcome tip convolution effects, which arise due to the finite size of tip apex and hamper imaging of larger non-planar objects. One approach to enhance the resolution is via tip functionalization, which revealed the atomic arrangement in Co clusters on NaCl-coated Au(111) surfaces[71]. Overcoming convolution effects by using atomically sharp tips and a detuning mode also recently permitted the atomic-scale analysis of 3D structures of Au nanoclusters on rutile TiO_2 by atomic force microscopy[72].

Although AC-STEM is extensively applied to study low-nuclearity catalysts, it is often challenging to discriminate information on the local environment. Like the determination of size, it requires sufficient phase contrast between metals and supports to study the interaction. Careful optimisation of imaging conditions is essential to minimise structural losses in beam-sensitive materials or atom displacement that lead to image artefacts like streaking or double recording of atoms[38]. In some well-defined systems, AC-STEM can provide powerful insights. For example, detailed analysis both along the [240] zone axis of the carrier and through tilting experiments demonstrated that the Ir atoms of homonuclear dimers were located on top of Fe columns and connected via oxygen bridges to α–Fe_2O_3[21]. A study of covalently bonded iron pairs in single-layer graphene sheets showed the metal species preferably reside in different defect sites, adopting distinct bonding configurations depending on the vacancy structure (**Fig. 4a**)[22]. Besides the location of small clusters and their

interaction with supports, analysis of measured atomic distances and intensities may provide information about their geometry. A study of Re on graphene showed that cluster sizes correlated with common tetrahedral and octahedral organizations[74]. In the analysis of platinum trimers supported on gamma-alumina, first-principle calculations identified the presence of hydroxyl ligands as the origin of the lack of agreement between measured and expected Pt-Pt bond distances, highlighting the possibility of imaging techniques to provide indirect indications for the coordination of ligands[75].

Advances in STEM approaches, for example permitting increased spatial resolution under low accelerating voltages, improved sensitivity to light atoms in the presence of heavy elements, and enabling the analysis of electron-beam-sensitive materials, promise to further extend the scope of atomic resolution imaging[76]. The fact that multiple geometries are observed even in relatively simple hosts emphasizes the likely diversity of coordination structures in low-nuclearity catalysts, which poses challenges even for determining the geometry of the minority species. Combined with the fact that species of distinct nuclearity may also be present, this calls for much greater automation of microscopy approaches to provide representative insights into the local environments. Other analytical techniques in TEM, especially electron energy loss spectroscopy, can provide highly complementary insights about the local environment, like quantitative elemental information and distinct chemical bonding environments and chemical states of atoms, with single-atom resolution[51,52]. The application of electron energy loss spectroscopy corroborated the Fe-N ratio of 4 determined by bulk spectroscopic techniques for iron atoms stabilized in graphene[64].

In cases where it is not straightforward to directly image the structure of catalytic materials, most experimental evidence comes from bulk spectroscopic methods. XAS techniques are the principal methods used to understand the structure of single atoms hosted on carbon-based materials[28,65,77]. However, the first coordination shell of metal atoms often comprises light elements (C, N, or O), which may substantially overlap in *R*-space, making it impossible to

tell them apart. Comparative EXAFS analysis using either wavelet or Fourier transforms identified the former as a powerful method for separating backscattering electrons permitting the discrimination of these atoms in *k*-space[65]. A big challenge lies in the fact that EXAFS data reflects an average signal of the composition, which hampers the assignment of characteristic spectroscopic fingerprints of individual structures in polydisperse samples[78]. A study of iron centres in carbons synthesized by pyrolysis clearly illustrated the complexity[77]. Investigation of a sample containing 0.5 wt% iron by EXAFS confirmed the absence of crystalline iron-based structures, evidencing characteristic Fe-N(O) and Fe-C interactions. Fitting of the EXAFS spectrum showed that the experimental data could correspond to either a square pyramidal or distorted octahedral coordination with the same accuracy (**Fig. 4b**). Comparatively, quantitative analysis of X-ray absorption near edge structure (XANES) spectra, which potentially offers greater sensitivity to the atom arrangement around the photo-absorber, revealed an unsatisfactory fit with DFT-derived FeN_xC_y structures. Instead, a good agreement emerged when a FeN_xC_y moiety based on a porphyrinic architecture was used either with two axially adsorbed oxygen molecules or with a single dioxygen molecule adsorbed side on (**Fig. 4c**).

Attempting to push boundaries in the design, researchers now look further than the first coordination sphere, with attempts to control the chemical identity of second nearest-neighbour sites and beyond[79]. Numerous examples exist for carbon-based materials, including by introducing distinct heteroatoms[80-82], creating vacancy or near-edge structures[83-87] in the vicinity of M-N_x centres, or constructing dual metal atom sites[88,89]. Most experimental evidence for the structures derives from XAS analyses, which requires a clear spectroscopic fingerprint. For example, electron density shifts from S to N atoms when a bond forms between them because of their distinct electronegativity. For this reason, two Fe-N contributions in the EXAFS spectra of Fe centres on S,N-doped carbons due to the resulting

asymmetry in bond lengths, contrasting to Fe atoms isolated on the N-doped analogue where only a single type is evident (**Fig. 4d**)[81].

The presence of metal clusters consisting of only a small number of atoms has been reported based on the observation of shortened metal-metal bonds compared to the bulk material[90]. In heteronuclear Co-Fe dual atom catalyst prepared by the sequential incorporation of Co and Fe atoms on nitrogen-doped carbon, the appearance of a new Co-Fe scattering path in the Co K-edge at 2.51 Å confirmed the interaction of the two metals[91]. However, structural disorder[22,78] and the easy oxidation[92,93] of subnanometric metal species can obscure second-shell M-M peaks complicating the structural analysis. Tackling the complexity of confirming the local environment relies heavily on DFT to establish preferred coordination sites of low-nuclearity species and the potential adsorption and effect of ligands. Extensive screening of the effects of the coordination motif in carbon-based hosts, and the adsorption of Cl ligands, highlighted the importance of controlling both properties to optimise the activity of Pt SACs in acetylene hydrochlorination (**Fig. 4e**)[94].

Electronic structure

Varying the size, composition, geometry, and atomic environment all influence the electronic structure of supported low-nuclearity metal species. Changes in electronic properties can originate for various reasons, including the variation of cluster orbital hybridization due to changes in the local coordination, charge transfer to and from the carrier, adsorbate-induced perturbations, and quantum size effects. The distinct resulting electronic structures may originate unique reactivity patterns compared to those observed for larger metal nanoparticles, emphasizing the importance of a precise understanding.

The intriguing question of how finite-sizes influence the electronic structure of metal clusters motivated several computational studies to understand the size dependence. To deconvolute the distinct contributing effects, early DFT calculations focused on the intrinsic changes in

free-standing Au and Pt clusters ranging from 13 to 1415 atoms and modelled as closed-shed cuboctahedra[95,96]. The results showed that clusters smaller than 560 atoms exhibited distinct characteristics from those of the bulk surface. At this point, the electronic states change from continuous to discrete, due to the confinement of the electron wavefunction. The main impact of reducing the size further resulted from the increasing fraction of undercoordinated surfaces associated with corner or edge atoms and their proximity to all surface atoms. Quantum size effects were only observed for Au and occur because of the specific *s*-electron shell structure, which leads to a gap around the Fermi level[96]. Considering the relative magnitudes of electron level spacings, the discreteness of the one-electron spectrum was only anticipated to significantly impact the bonding in the smallest clusters (<10 atoms).

Several high-energy spectroscopy methods, most commonly X-ray photoelectron spectroscopy (XPS) and XANES, can provide direct insights into the electronic structures of low-nuclearity catalysts. Some of the first systematic insights came from XPS analysis, probing the kinetic energy of photoelectrons ejected from occupied states, of mass-selected clusters on distinct supports, for example Pt_n/SiO_2 (n = 1-6)[97], Pd_n/TiO_2 (n = 1, 2, 4, 7, 10, 16, 20, and 25)[98], or Pt_n/Al_2O_3 (n = 1, 2, 4, 7, 10, 14, 18)[99]. These studies showed that the core-level binding energy of Pt 4*f* and Pd $3d_{5/2}$ electrons fluctuate and were typically shifted to positive values relative to the bulk metal. The precise interpretation of these shifts is complex as several effects could impact the initial or final states of the photoemission process[100]. Besides changes in the electronic structure resulting from distinct geometries of low-nuclearity species or chemical bonding to host materials, quantum size effects can also alter the initial state but the exact contribution is still not well understood. Final state effects, primarily relate to size-dependent core-hole screening and charging effects, can also be significant, especially on insulating hosts.

Taking the effect of size-dependent charging into account, analysis of the results observed for the Pd/TiO_2 catalysts identified one of the first correlations between the electronic structure

and the performance of low-nuclearity metals, showing that the CO oxidation activity increased with a lower than expected occupancy of the 3*d* orbitals[98]. Calculations of the initial state XPS shift found that this primarily depended on the hybridization of the cluster because it originated from the occupation of Pd 4*d* orbitals in the Pd clusters[100]. The importance of a precise configuration of the metal species on the carrier was highlighted by a later study of atomically-dispersed Pd_n (n = 1-3) species anchored on graphitic carbon nitride[22]. Two distinct positively charged palladium species, tentatively assigned to Pd^{4+} (338.5 eV) and Pd^{2+} (336.9 eV) based on formal charges, were identified in all samples, and the Pd^{2+}:Pd^{4+} ratio increased with the size of the palladium species, evidencing a reduced degree of oxidation (**Fig. 5a**). A good agreement was reported with the XPS shifts simulated along molecular dynamics trajectories, which showed that the degree of oxidation of Pd atoms depended on their location (surface versus subsurface) in the carbon nitride structure.

Valence photoemission spectroscopy has also been applied to provide a direct measure of the changes in the density of 3*d* states in single-atom Ag-Cu alloy in which Cu atoms are isolated within a Ag matrix (**Fig. 5b**)[101]. Comparison of the results with projected density of state calculations uncovered a unique free-atom like electronic structure on Cu resulting from weak wavefunction mixing between minority and majority elements. Calculations identified a general correlation between the difference in adsorption energies of *s*- and *p*-block elements on the isolated Cu site in the dilute Ag-Cu alloy compared to bulk Cu and the difference in electronegativity between Cu and the respective adsorbates. A sharp peak near the Fermi level in their atom projected *d*-band density of states was also identified for palladium atoms in a separate theoretical study of Ag-Pd and Au-Pd alloys[102]. Although favourable energetics were demonstrated in the dissociation of nitric acid and the hydrogenation of acetylene, the findings showed that reactivity could not easily explained by the scaling trends usually observed on transition metal alloy surfaces.

XANES spectroscopy is also commonly applied to probe two key features of the electronic structure of supported metal clusters. The energy required to excite an electron from the core level into the lowest unoccupied orbital determines the energy of the absorption onset, or edge, while information about the density of unoccupied states and the transition probabilities to them from the initial core level is reflected by the intensity of the absorption maximum (also known as the white-line intensity) that often appear close to the edge. As with XPS, size effects on screening and relaxation in the XANES core-hole final state can significantly impact the binding energy of core orbitals. Comparison of the XANES spectra of a series of size-selected Pt_n/SiO_2 materials identified increasing shifts in the Pt L_3 edge relative to bulk Pt with decreasing cluster size, suggesting that the clusters are oxidized. However, analysis by XPS showed that they are not[103]. This discrepancy was attributed to the development of a band gap and localization of empty state wave functions in small clusters, which affect both the energy and density of the unoccupied states that are populated in XANES. Increasing band gaps with decreasing size of metal species have been previously evidenced by UV photoelectron spectroscopy (UPS)[97,99]. XANES has been widely used to investigate the properties of SACs, and this raises the obvious question of how reliable it is to interpret the results by reference to bulk standards. To go beyond this, a recent study of supported Cu_4O_x and Cu_5O_y clusters showed that fitting the experimental spectrum to calculated spectra of supported clusters can provide a better agreement, identifying the partial reduction of the clusters with increasing temperature, whereas in some cases it was impossible to obtain a good fit to Cu_2O and CuO reference spectra[104].

Several other complementary techniques can potentially provide insight into the electronic structure of low-nuclearity catalysts. Because small structural variations may have tremendous effects, the direct visualization of the bonding and electronic configuration with atomic resolution by AC-STEM is highly desirable. Most developments in this direction have been made in the field of two-dimensional materials such as graphene. By studying the fine

structure of electron energy loss spectra combined with ab initio calculations it was possible to distinguish between distinct electronic structures of isolated Si substitutional defects in single-layer graphene depending on the number of direct bonds they form with the host lattice (**Fig. 5c**)[103]. This prompted several studies examining the spectroscopic signatures of *p*- and *n*-type doping, for example with N, B, or P in graphene[106-108]. For transition metal atoms, analysis of EELS fine structure has focused on comparing the intensity of distinct contributions to the L edge with respect to bulk metal or metal oxide references[53,54]. Rapid progress in instrumentation has also recently permitted the use of differential phase contrast imaging for directly mapping the local charge density in catalytic materials with sub-ångström resolution[109-111]. By studying Au atoms on an amorphous carbon host it was possible to spatially resolve the electric field distribution within single atoms[112], demonstrating exciting potential to study the impact of the local environment. Another technique with the potential to atomically resolve the surface density of states of low-nuclearity species in suitable samples is STM imaging combined with scanning tunnelling spectroscopy. In the analysis of single-atom alloys, palladium atoms isolated in a copper lattice were found to be almost electronically identical to their host atoms[113]. The study of In-Sn bimetallic chains on a single crystal silicon surface identified the preferential formation of In-Sn dimers stabilized by charge transfer to neighbouring In-In dimers, which induces the emergence of localized electronic states at, or slightly above, the Fermi level[114].

An area where tailoring the electronic structure has been actively pursued is in the design of single-atom electrocatalysts, with approaches mainly targeting the optimisation of charge density on the metal centres to optimise adsorption strengths of intermediates[77,115]. Several correlations have been drawn between the chemical identity of the central metal atom and the performance based on DFT comparisons of SACs of various transition metals in equivalent coordination sites[89,116,117]. Besides, adjusting the coordination environment of central metal ions is another effective strategy to tune the electronic structure. Integrated approaches,

typically combining dedicated syntheses to prepare carriers with specific coordination sites with XAS, XPS, and DFT, have highlighted the huge changes in electronic and geometric structure experienced after the rehybridization of metal orbitals[118-120]. Concomitantly, the interaction with metal clusters can significantly modify the electronic properties of neighbouring carrier atoms[122,123]. Distinct electronic structures resulting from changes in the carrier phase due to the presence of single-atom dopants have been linked to enhanced performance in the hydrogen evolution reaction[124,125]. Compared to SACs, only a few relations between the electronic structure and reactivity have been established for other low-nuclearity species, mainly limited to metal dimers[88,126]. Recently, the assembly of single-atom-thick layers of Pd-Co alloys, containing metal centres that are zero coordinate in one dimension but highly coordinated within the plane, was shown to yield high stability and activity for the electrochemical reduction of oxygen or formic acid[127]. Based on analysis by XANES and XPS, this was attributed to the oriented splitting of valence/empty *d*- and *p*-bands into lower-energy bands in the *x*-*y* plane and a higher-energy band in the *z* direction (**Fig. 5d**). The splitting was not observed in the directionless bonding of nanoparticles of the Pd-Co alloy or due to the weak Pd-Pd interaction in single-atom layers of palladium alone.

Location and structural dynamics

Effects of 3D catalyst architecture

Knowledge of the location and corresponding spatial distribution of low-nuclearity metal species on carrier materials is critical for being able to quantify the utilization of the atoms of the minority element and for understanding both their interaction and interconnected structural dynamics. Although a common target of developing catalysts integrating low-nuclearity species is to enable full metal utilization, this may not be achieved if the active phase is partially or fully incorporated into the subsurface or bulk of the carrier, and thus still unable to participate in the reaction. Direct synthesis approaches where metals are introduced

during carrier syntheses could be particularly prone to this, but percolation of metal species can also occur when using post-synthetic routes[38]. Surprisingly, the assessment of important characteristics pertaining to the location of low-nuclearity species, including the surface metal concentration, proximity of metal species, and accessibility within porous carriers, has received limited attention.

Quantitative measurement of the number of surface sites of a given kind in catalytic materials is fundamental because this information is needed to estimate the turnover frequency, which is a widely used measure of comparative activity. However, the application of selective chemisorption techniques, standardly used to quantify the degree of dispersion of supported metal nanoparticles, cannot be readily extended to small metal clusters because the coordination of typical probe molecules as hydrogen or carbon monoxide differs from that of bulk metal surfaces[128]. As discussed concerning nuclearity determination, SACs comprise a special case where the adsorption of CO can potentially probe the number of surface metal atoms. Due to the sensitivity of the C–O stretch frequency to different metals and binding sites, quantitative analysis is typically facilitated on single-crystal surfaces[129]. Besides, the specific electronic structure may preclude its use for the study of certain low-nuclearity catalysts[22]. Nonetheless, with careful analysis and appropriate monitoring to ensure that the absence of adsorbate-induced reconstruction, strong correlations have been derived between the site fractions of Rh, Pt, and Ir single atoms estimated by CO chemisorption and the performance in distinct applications[130-132]. Alternatively, the fraction of surface atoms can be roughly approximated by comparing the global elemental composition with the metal content determined by a more surface-sensitive technique such as XPS[38,133] or low energy ion scattering[134].

The distance between supported metal species can originate intricate, often not yet understood effects in low-nuclearity catalysts. Variation of the size and coverage of Pt clusters on carbons evidenced a decisive impact on the activity in the oxygen reduction reaction that was

tentatively attributed to changes in the overlap of the electric double layer[135]. Recent progress in the design of double or triple atom catalysts, where synergetic effects between two or three atoms of the same or different chemical identity enhance the performance, highlights the challenges associated with the precise determination and control of atom proximity has been scarcely addressed[136,137]. Besides impacting the activity and selectivity, the distance between metal species also determines the collective properties that affect the stability by influencing the propensity towards sintering or redispersion[138,139]. Interactions between adjacent metal species become more significant upon shortening the distance between them, and thus increasing the mass loading and associated surface density while preserving the size of metal species is a common strategy to detect them, although control over proximity is random. For larger nanoparticles, electron tomography has been elegantly exploited to provide precise 3D information about the location in porous supports[139]. For single-atom catalysts, the proximity has been manually estimated by measuring the distance between species in standard micrographs[21,140], but can only provide a tentative picture except for the careful analysis of crystalline hosts. Other approaches, such as the identification of M-M bonds by EXAFS or of bridged adsorption of CO can confirm the formation of metal clusters, but not intercluster distances.

Even if all the metal species reside on the carrier surface, another consideration that has been little addressed in the design of low-nuclearity catalysts is their accessibility depending on their 3D spatial environment. Carbons-based materials are pervasive carriers, especially in electrocatalysis, due to the various possibilities to introduce a wide variety of heteroatoms and tailor their porosity and conductivity[8]. Despite often exhibiting high microporosity, the question of the potential effects of metal pore confinement on the utilisation of supported metal species has been virtually neglected. Accessibility constraints, where reactant or intermediate molecules are too bulky to diffuse to active sites situated within pores or similar dimensions, are well-known in the development of other microporous catalysts, such as

zeolites[141]. An improved understanding of the effects of the location of metal species within the pore networks of carrier materials, which could be approached by spatially resolving the 3D architecture of the catalyst or through test reactions using substrates of different size, will be of great value for determining the effective metal utilisation in future work.

Dynamic effects and property evolution

The ability to stabilize low-nuclearity metals was fundamental to their integration and exploitation as catalysts within carrier materials. The challenges in predicting the intrinsic stability have been highlighted for the case of SACs[142]. If the free-energy change is negative, nanoparticles may spontaneously disperse into low-nuclearity species of a given type (thermodynamic stability), but low-nuclearity species can be trapped even if the free energy is positive by increasing the aggregation barrier sufficiently to prevent sintering (kinetic stability). Several examples of SACs with higher thermal stability than their supported nanoparticle analogues have been reported[143-145].

Independently of whether low-nuclearity metals are kinetically or thermodynamically stabilized on carrier materials, their structure (location, geometry, coordination environment, electronic) may evolve under reaction conditions, which may be induced by various effects including changes in the energetics due to, for example, interactions with reactants or intermediates and/or structural transformations of the carrier. The possibility of using SACs as model systems to understand these effects has prompted great interest in the application of in situ/operando techniques, especially XAS, STM, and infrared[146]. Direct visualization by STM revealed the migration of iridium adatoms deposited on a model $Fe_3O_4(001)$ surface from the surface to the subsurface upon thermal annealing, becoming inactive for adsorption (**Fig. 6a**)[66]. Changes in location upon exposure to various environmental conditions may also solely occur on the surface and may be reversible. A combined in situ atomic resolution and spectroscopy analysis of Pt atoms on a TiO_2 anatase carrier showed that the Pt species could

adopt a range of local coordination environments (**Fig. 6b**), which strongly influenced the chemical reactivity[147]. Theoretically, DFT can provide valuable insights into the energetically preferred locations and structures of low-nuclearity species at elevated temperatures and in the presence of potential adsorbates[94,147]. Nonetheless, static DFT cannot account for nonconventional, relatively short-lived species, sometimes encountered in highly dynamic systems. Recently, changes in the surface concentration of atomically-dispersed copper species due to percolation into the carbon nitride host were effectively quantified by kMC simulations (**Fig. 6c**)[148], obtaining a direct correlation with the catalyst activity.

When supported on carriers integrating multidentate coordination sites several energetically favourable stabilization states may coexist with minimal barriers between them, permitting interchange between them. The wide range of surface and subsurface configurations of palladium atoms, dimers, and trimers on graphitic carbon nitride was illustrated by molecular dynamics simulations (**Fig. 6d**)[22]. The possibility for metal species to change the coordination with the host while preserving their nuclearity is central to the concept of adaptative coordination, where the metal-host bonding can vary in response to the reaction requirements. In Suzuki coupling, DFT calculations showed that the flexible lattice of graphitic carbon nitride enables an almost continuously variable coordination pattern of palladium to the host during the catalytic cycle, originating high stability to deactivation by metal leaching[149]. Similar localized adaptions of the coordination environment have been reported based on operando characterization for Rh single atoms on TiO_2 during the reverse water gas shift reaction[150], and for Co and Ru single-atom electrocatalysts on nitrogen-doped carbons for hydrogen[151] and oxygen[152] evolution, respectively.

Besides variations due to migration or the adsorption of ligands, metal atoms and clusters may change their nuclearity by sintering into larger or re-dispersion into smaller species, respectively. Such restructuring is well known for catalysts based on nanoparticles and has been extensively studied with advanced microscopy and spectroscopy techniques[153,154].

Changes in nuclearity can have beneficial or deleterious effects on performance, depending on whether the initial state is optimal. They may be progressive and irreversible, for example, the transformation of nanoparticles into single atoms or vice versa[94,155,156], in which case the impact can be readily detected by ex-situ techniques. On the other hand, they may occur discreetly and transiently under reaction conditions, requiring the use of operando methods to understand the factors controlling them[157,158]. The dynamic and reversible formation of active sites under reaction conditions in known in diverse systems, such as Cu ions in zeolites during selective catalytic reduction[158] and Au ions on oxides during CO oxidation comprising prominent examples[159]. The role of adsorbates in inducing the mobility among otherwise stable adatoms has been directly visualized by STM for Pt/Fe_3O_4 (**Fig. 6e**)[160]. A recent theoretical study also highlighted the nonconventional behaviour that could be expected for sub-nanometre Au clusters, predicting the occurrence of solid-to-liquid phase transitions when taking entropy effects into account[161].

Comparatively, the stability of bi- and multimetallic low-nuclearity systems has received less attention. Besides changes in size, segregation phenomena can occur for supported metal alloy nanoparticles[162]. The stability of single-atom alloys has been systematically evaluated by DFT, using the segregation and aggregation energies as descriptors of the mobility of dopant atoms. The interaction with adsorbates such as CO induced dopant atom segregation into the surface layer for a wide range of compositions, whereas aggregation and island formation could be promoted or inhibited depending on alloy constitution and CO coverage[163]. In bimetallic systems, the treatment of Au nanoparticles (>70 nm in diameter) supported on carbon with an aqueous solution of H_2PtCl_6 resulted in the full dispersion of both metals as isolated atoms (**Fig. 6f**)[164]. Investigation of the effect of various synthetic parameters showed that the re-dispersion likely follows a chlorine-mediated mechanism, promoted by a high redox potential of the second metal and high Cl:Au ratios. Interestingly, the bimetallic single-atom system exhibited greatly enhanced resistance to sintering compared

to single Au atoms on the same carrier, indicative of a higher barrier to diffusion and aggregation in the presence of Pt.

Evolution of the geometric structure directly impacts the electronic configuration of low-nuclearity catalysts and monitoring the variation in charge state is also critical for the establishment of property-function relationships. The flexibility of low-nuclearity species to change charge state may be a prerequisite to fulfilling the requirements of the catalytic cycle. If immobilized too strongly, they may be inactive, and thus controlling the interaction with supports is crucial. Stepwise exploration of reaction steps in CO oxidation by STM and XPS permitted detailed insight into the changes in the charge state of Au atoms supported on CuO, confirming the role of charge transfer from the support in tuning the activity[165]. A theoretical analysis of Pt atoms on CeO_2 identified the possible coexistence of several well-defined and dynamically interconnected charge and oxidation states (**Fig. 6g**), demonstrating the oversimplification of the current static picture of electronic structures[166].

Discriminating the effect of dynamic structural changes is complex, and inadequate characterization can introduce confusion in the interpretation of results[92]. The development of suitable cells to enable correlated approaches, for example combining XAS and TEM, can provide useful insights for interpreting of the results[167]. Due to the ease of detection, most environmental TEM studies to date have focused on Pt or Ir, and dedicated efforts to visualize the transformations of lighter elements under reactive gases will be valuable in the future[168]. The timescales of dynamic phenomenon also need to be carefully examined relative to the time resolution of the techniques applied, which may be insufficient to capture all relevant underlying structural changes.

Outlook

The last decade witnessed unprecedented progress and enormous creativity in developing catalytic materials integrating metal species with controlled atomicity and composition.

Growing understanding increasingly points to the remarkably singular properties of the corresponding active species, making precision design ever-more fascinating but incredibly complex to achieve. In the characterization of crucial structural features, experimentalists are working at the frontiers of the resolution of existing techniques. Because of the lack of tools to control and discriminate key properties, catalyst discovery often relies on empirical screening guided by the influence of varying the synthetic parameters on the performance. Concepts targeting the preparation of model architectures on practical 3D carriers combined with the systematic assessment of characteristic signatures will be valuable to complement the widespread culture of only reporting high-performing functional materials.

The absence of general routes for the preparation of low-nuclearity catalysts on practical carriers calls for more intensive research into the synthesis. The study of the adsorption of metal precursors on carriers with well-defined surface anchoring sites, their subsequent decomposition, and behaviour upon exposure to distinct reactive environments will provide an improved mechanistic understanding of the factors influencing the nuclearity and stability of the introduced metal species. As highlighted in this review, the presence of ligands and other surface species can strongly influence the dispersion and mobility of supported metals and may offer valuable paths for tailoring the preferred structure.

Polydispersity, whether arising from a distribution of coordination sites on the carrier or structural evolution under reaction conditions, calls for careful interpretation of experimental results. In this direction, recent perspectives have discussed the scope of methods to analyse the uniformity of site distributions of atomically-dispersed platinum group metals based on band frequencies and widths of adsorbed carbon monoxide and temperature programmed desorption studies[169,170]. A possible approach is to reduce the metal loading to selectively titrate the most stable configurations and characteristic signatures of metal species on a given carrier, but this is most suited for crystalline carriers with a lower diversity of anchoring sites and is simplified for single atoms where the nuclearity can be verified more readily. Breaking

away from the traditional concept of designing a single active site, the use of statistical active-site distributions, whether experimentally of computationally defined, may be more appropriate for the establishment of structure-performance relations over some catalytic systems. While operando techniques are widely consulted to provide insights into dynamic effects, intrinsic limitations of the approaches are often intensified in reactive environments. Further progress in improving the time and spatial resolution will be pivotal to develop a deeper appreciation of system fluxionality.

Low-nuclearity species provide an ideal arena for theory, which is pushing forward understanding and concepts associated with these advanced systems in an unprecedented manner. The theoretical findings provide extensive inspiration for the synthesis of novel catalytic systems, which will serve the dual purpose of validating the simulations. The site diversity in many carriers combined with the possible presence of adsorbates and dynamic effects calls for extensive screening of possible structures combining DFT with kinetic Monte Carlo and molecular dynamics simulations. The results provide rich datasets to map onto experimental data, potentially using emerging digital tools. The latter are bound to originate disruptive future advances, which will be accelerated by increasing familiarity and progress in algorithm development and deployment.

Until we have improved comprehension and control over the structure of local atomic environments across multiple scales, our ability to innovate energy-efficient chemical processes will still rely on serendipitous findings. The design of catalysts in technically-relevant forms poses a further challenge. Increased emphasis is required on scale up to maximize the potential for commercialisation of these advanced materials.

References

1. Mitchell, S., Qin, R., Zheng, N., Pérez-Ramírez J., Nanoscale engineering of catalytic materials for sustainable technologies. *Nat. Nanotechnol.* **16**, 129-139 (2020).
2. Chng, L. L., Erathodiyil, N. & Ying, J. Y. Nanostructured catalysts for organic transformations. *Acc. Chem. Res.* **46**, 1825-1837 (2013).
3. Mistry, H., Varela, A. S., Kühl, S., Strasser, P. & Cuenya, B. R. Nanostructured electrocatalysts with tunable activity and selectivity. *Nat. Rev. Mater.* **1**, 1-14 (2016).
4. Xu, C., Anusuyadevi, P. R., Aymonier, C., Luque, R. & Marre, S. Nanostructured materials for photocatalysis. *Chem. Soc. Rev.* **48**, 3868-3902 (2019).
5. Liu, L. & Corma, A. Confining isolated atoms and clusters in crystalline porous materials for catalysis. *Nat. Rev. Mater.* doi: 10.1038/s41578-020-00250-3 (2020).
6. Tyo, E. C. & Vajda, S. Catalysis by clusters with precise numbers of atoms. *Nat. Nanotechnol.* **10**, 577-588 (2015).
7. Gates, B. C. Supported metal clusters: synthesis, structure, and catalysis. *Chem. Rev.* **95**, 511-522 (1995).
8. Kaiser, S. K., Chen, Z., Faust Akl, D., Mitchell, S. & Pérez-Ramírez, J. Single-atom heterogeneous catalysts across the periodic table. *Chem. Rev.* **120**, 11703-11809 (2020).
9. Wang, A., Li, J. & Zhang, T. Heterogeneous single-atom catalysis. *Nat. Rev. Chem.* **2**, 65-81 (2018).
10. Mitchell, S., Vorobyeva, E. & Pérez-Ramírez, J. The multifaceted reactivity of single-atom heterogeneous catalysts. *Angew. Chem. Int. Ed.* **57**, 15316-15329 (2018).
11. Dong, C. et al. Supported metal clusters: fabrication and application in heterogeneous catalysis. *ACS Catal.* **10**, 11011-11045 (2020).
12. Böhme, D. K. & Schwarz, H. Gas-phase catalysis by atomic and cluster metal ions: the ultimate single-site catalysts. *Angew. Chem. Int. Ed.* **44**, 2336-2354 (2005).
13. Zhai, H. & Alexandrova, A. N. Fluxionality of catalytic clusters: when it matters and how to address it. *ACS Catal.* **7**, 1905-1911 (2017).
14. Rong, H., Ji, S., Zhang, J., Wang, D. & Li, Y. Synthetic strategies of supported atomic clusters for heterogeneous catalysis. *Nat. Commun.* **11**:5884 (2020).
15. Pan, Y. H., Sohlberg, K. & Ridge, D. P. Reactions of cobalt ions $Co_{1\text{-}4}^{+}$ and $Co_4(CO)^{n+}$ with cyclohexane: CH activation as a function of cluster size and ligand substitution. *J. Am. Chem. Soc.* **113**, 2406-2411 (1991).
16. Vajda, S. & White, M. G. Catalysis applications of size-selected cluster deposition. *ACS Catal.* **5**, 7152-7176 (2015).

17. Xu, Z. et al. Size-dependent catalytic activity of supported metal clusters. *Nature* **372**, 346-348 (1994).
18. Goellner, J. F., Guzman, J. & Gates, B. C. Synthesis and structure of tetrairidium clusters on TiO_2 powder: characterization by infrared and extended X-ray absorption fine structure spectroscopies. *J. Phys. Chem. B* **106**, 1229-1238 (2002).
19. Imaoka, T. et al. Platinum clusters with precise numbers of atoms for preparative-scale catalysis. *Nat. Commun.* **8**:688 (2017).
20. Tian, S. et al. Carbon nitride supported Fe_2 cluster catalysts with superior performance for alkene epoxidation. *Nat. Commun.* **9**:2353 (2018).
21. Zhao, Y. et al. Stable iridium dinuclear heterogeneous catalysts supported on metal-oxide substrate for solar water oxidation. *Proc. Nat. Acad. Sci.* **115**, 2902-2907 (2018).
22. Vorobyeva, E. et al. Atom-by-atom resolution of structure-function relations over low-nuclearity metal catalysts. *Angew. Chem. Int. Ed.* **58**, 8724-8729 (2019).
23. Liu, S. et al. Stabilizing single-atom and small-domain platinum via combining organometallic chemisorption and atomic layer deposition. *Organometallics* **36**, 818-828 (2017).
24. Detavernier, C., Dendooven, J., Sree, S. P., Ludwig, K. F. & Martens, J. A. Tailoring nanoporous materials by atomic layer deposition. *Chem. Soc. Rev.* **40**, 5242-5253 (2011).
25. Sun, S. et al. Single-atom catalysis using Pt/graphene achieved through atomic layer deposition. *Sci. Rep.* **3**, 1775 (2013).
26. Yan, H. et al. Single-atom Pd_1/graphene catalyst achieved by atomic layer deposition: remarkable performance in selective hydrogenation of 1,3-butadiene. *J. Am. Chem. Soc.* **137**, 10484-10487 (2015).
27. Cheng, N. et al. Platinum single-atom and cluster catalysis of the hydrogen evolution reaction. *Nat. Commun.* **7**:13638 (2016).
28. Yan, H. et al. Atomic engineering of high-density isolated Co atoms on graphene with proximal-atom controlled reaction selectivity. *Nat. Commun.* **9**:3197 (2018).
29. Yan, H. et al. Bottom-up precise synthesis of stable platinum dimers on graphene. *Nat. Commun.* ***8***:1070 (2017).
30. Zhang, L. et al. Atomic layer deposited Pt-Ru dual-metal dimers and identifying their active sites for hydrogen evolution reaction. *Nat. Commun.* **10**:4936 (2019).

31. Platero-Prats, A. E. et al. Bridging zirconia nodes within a metal–organic framework via catalytic Ni-hydroxo clusters to form heterobimetallic nanowires. *J. Am. Chem. Soc.* **139**, 10410-10418 (2017).
32. Wei, Y. S. et al. Fabricating dual-atom iron catalysts for efficient oxygen evolution reaction: a heteroatom modulator approach. *Angew. Chem. Int. Ed.* **59**, 16013-16022 (2020).
33. Ji, S. et al. Confined pyrolysis within metal–organic frameworks to form uniform Ru_3 clusters for efficient oxidation of alcohols. *J. Am. Chem. Soc.* **139**, 9795-9798 (2017).
34. Zhou, Y. et al. Revealing of active sites and catalytic mechanism in N-coordinated Fe, Ni dual-doped carbon with superior acidic oxygen reduction than single-atom catalyst. *J. Phys. Chem. Lett.* **11**, 1404-1410 (2020).
35. Wu, H. B., Xia, B. Y., Yu, L., Yu, X. Y. & Lou, X. W. D. Porous molybdenum carbide nano-octahedrons synthesized via confined carburization in metal-organic frameworks for efficient hydrogen production. *Nat. Commun.* **6**:6512 (2015).
36. Xu, Y. T. et al. Cage-confinement pyrolysis route to ultrasmall tungsten carbide nanoparticles for efficient electrocatalytic hydrogen evolution. *J. Am. Chem. Soc.* **139**, 5285-5288 (2017).
37. Tada, M., Taniike, T., Kantam, L. M. & Iwasawa, Y. Chiral self-dimerization of vanadium complexes on a SiO_2 surface: the first heterogeneous catalyst for asymmetric 2-naphthol coupling. *Chem. Commun.* 2542-2543 (2004).
38. Chen, Z. et al. Stabilization of single metal atoms on graphitic carbon nitride. *Adv. Funct. Mater.* **27**, 1605785 (2017).
39. Zhou, P. et al. Synergetic interaction between neighboring platinum and ruthenium monomers boosts CO oxidation. *Chem. Sci.* **10**, 5898-5905 (2019).
40. Dai, S. et al. Platinum-trimer decorated cobalt-palladium core-shell nanocatalyst with promising performance for oxygen reduction reaction. *Nat. Commun.* **10**:440 (2019).
41. Wang, J. et al. Design of N-coordinated dual-metal sites: a stable and active Pt-free catalyst for acidic oxygen reduction reaction. *J. Am. Chem. Soc.* **139**, 17281-17284 (2017).
42. Yang, Y. et al. O-coordinated W-Mo dual-atom catalyst for pH-universal electrocatalytic hydrogen evolution. *Sci. Adv.* **6**, p.eaba6586 (2020).
43. Baldansuren, A., Dilger, H., Eichel, R. A., van Bokhoven, J. A. & Roduner, E. Interaction and reaction of ethylene and oxygen on six-atom silver clusters supported on LTA zeolite. *J. Phys. Chem. C* **113**, 19623-19632 (2009).

44. Fortea-Pérez, F. R. et al. The MOF-driven synthesis of supported palladium clusters with catalytic activity for carbene-mediated chemistry. *Nat. Mater.* **16**, 760 (2017).
45. Liu, L. et al. Generation of subnanometric platinum with high stability during transformation of a 2D zeolite into 3D. *Nat. Mater.* **16**, 132-138 (2017).
46. Uzun, A., Ortalan, V., Browning, N. D. & Gates, B. C. Site-isolated iridium complexes on MgO powder: individual Ir atoms imaged by scanning transmission electron microscopy. *Chem. Commun.* 4657-4659 (2009).
47. Allard, L. F. et al. Evolution of gold structure during thermal treatment of Au/FeO_x catalysts revealed by aberration-corrected electron microscopy. *J. Electron Microsc.* **58**, 199-212 (2009).
48. Lu, Z. et al. An isolated zinc–cobalt atomic pair for highly active and durable oxygen reduction. *Angew. Chem. Int. Ed.* **131**, 2648-2652 (2019).
49. Yang, Y. et al. Deciphering chemical order/disorder and material properties at the single-atom level. *Nature* **542**, 75-79 (2017).
50. Zhou, J. et al. Observing crystal nucleation in four dimensions using atomic electron tomography. *Nature* **570**, 500-503 (2019).
51. Suenaga, K. et al. Element-selective single atom imaging. *Science* **290**, 2280-2282 (2000).
52. Senga, R. & Suenaga, K. Single-atom electron energy loss spectroscopy of light elements. *Nat. Commun.* **6**:7943 (2015).
53. Resasco, J. et al. Uniformity is key in defining structure-function relationships for atomically dispersed metal catalysts: The case of Pt/CeO_2. *J. Am. Chem. Soc.* **142**, 169-184 (2019).
54. Lin, L. et al. Atomically dispersed Ni/α-MoC catalyst for hydrogen production from methanol/water. *J. Am. Chem. Soc.* **143**, 309-317 (2020).
55. Jiang, K. et al. Transition-metal single atoms in a graphene shell as active centers for highly efficient artificial photosynthesis. *Chem* **3**, 950-960 (2017).
56. Perea, D. E. et al. Determining the location and nearest neighbours of aluminium in zeolites with atom probe tomography. *Nat. Commun.* **6**:7589 (2015).
57. Schmidt, J. E., Oord, R., Guo, W., Poplawsky, J. D. & Weckhuysen, B. M. Nanoscale tomography reveals the deactivation of automotive copper-exchanged zeolite catalysts. *Nat. Commun.* **8**:1666 (2017).

58. Kovarik, L. et al. Transformation of active sites in Fe/SSZ-13 SCR catalysts during hydrothermal aging: a spectroscopic, microscopic, and kinetics study. *ACS Catal.* **7**, 2458-2470 (2017).
59. Wang, X. et al. Interpreting nanovoids in atom probe tomography data for accurate local compositional measurements. *Nat. Commun.* **11**:1022 (2020).
60. Ding, K. et al. Identification of active sites in CO oxidation and water-gas shift over supported Pt catalysts. *Science* **350**, 189-192 (2015).
61. DeRita, L. et al. Catalyst architecture for stable single atom dispersion enables site-specific spectroscopic and reactivity measurements of CO adsorbed to Pt atoms, oxidized Pt clusters, and metallic Pt clusters on TiO_2. *J. Am. Chem. Soc.* **139**, 14150-14165 (2017).
62. Aleksandrov, H. A., Neyman, K. M., Hadjiivanov, K. I. & Vayssilov, G. N. Can the state of platinum species be unambiguously determined by the stretching frequency of an adsorbed CO probe molecule? *Phys. Chem. Chem. Phys.* **18**, 22108-22121 (2016).
63. Deng, D. et al. A single iron site confined in a graphene matrix for the catalytic oxidation of benzene at room temperature. *Sci. Adv.* **1**, e1500462 (2015).
64. Chung, H. T. et al. Direct atomic-level insight into the active sites of a high-performance PGM-free ORR catalyst. *Science* **357**, 479-484 (2017).
65. Fei, H. et al. General synthesis and definitive structural identification of MN_4C_4 single-atom catalysts with tunable electrocatalytic activities. *Nat. Catal.* **1**, 63 (2018).
66. Jakub, Z. et al. Local structure and coordination define adsorption in a model Ir_1/Fe_3O_4 single-atom catalyst. *Angew. Chem. Int. Ed.* **58**, 13961-13968 (2019).
67. Yang, S. Z. et al. Rhenium-doped and stabilized MoS_2 atomic layers with basal-plane catalytic activity. *Adv. Mater.* **30**, 1803477 (2018).
68. Lucci, F. R. et al. Selective hydrogenation of 1,3-butadiene on platinum–copper alloys at the single-atom limit. *Nat. Commun.* **6**:8550 (2015).
69. Piednoir, A. et al. Atomic resolution on small three-dimensional metal clusters by STM. *Surf. Sci.* **391**, 19-26 (1997).
70. Isomura, N., Wu, X. & Watanabe, Y. Atomic-resolution imaging of size-selected platinum clusters on TiO_2(110) surfaces. *J. Chem. Phys.* **131**, 164707 (2009).
71. Schouteden, K. et al. Probing the atomic structure of metallic nanoclusters with the tip of a scanning tunneling microscope. *Nanoscale* **6**, 2170-2176 (2014).

72. Adachi, Y., Sugawara, Y. & Li, Y. J. Atomic scale three-dimensional Au nanocluster on a rutile TiO_2(110) surface resolved by atomic force microscopy. *J. Phys. Chem. Lett.* **11**, 7153-7158 (2020).
73. He, Z. et al. Atomic structure and dynamics of metal dopant pairs in graphene. *Nano Lett.* **14**, 3766-3772 (2014).
74. Miramontes, O. et al. Ultra-small rhenium clusters supported on graphene. *Phys. Chem. Chem. Phys.* **17**, 7898-7906 (2015).
75. Sohlberg, K., Rashkeev, S., Borisevich, A. Y., Pennycook, S. J. & Pantelides, S. T. Origin of anomalous Pt–Pt distances in the Pt/alumina catalytic system. *ChemPhysChem* **5**, 1893-1897 (2004).
76. Xu, M., Li, A., Gao, M. & Zhou, W. Single-atom electron microscopy for energy-related nanomaterials. *J. Mater. Chem. A* **8**, 16142-16165 (2020).
77. Zitolo, A. et al. Identification of catalytic sites for oxygen reduction in iron-and nitrogen-doped graphene materials. *Nat. Mater.* **14**, 937-942 (2015).
78. Feng, K. et al. Single atoms or not? The limitation of EXAFS. *Appl. Phys. Lett.* **116**, 191903 (2020).
79. Sun, T. et al. Design of local atomic environments in single-atom electrocatalysts for renewable energy conversions. *Adv. Mater.* **33**, 2003075 (2020).
80. Shen, H. et al. Synergistic effects between atomically dispersed Fe−N−C and C−S−C for the oxygen reduction reaction in acidic media. *Angew. Chem. Int. Ed.* **56**, 13800-13804 (2017).
81. Li, Q. et al. Fe isolated single atoms on S, N codoped carbon by copolymer pyrolysis strategy for highly efficient oxygen reduction reaction. *Adv. Mater.* **30**, 1800588 (2018).
82. Chen, Y. et al. Enhanced oxygen reduction with single-atomic-site iron catalysts for a zinc-air battery and hydrogen-air fuel cell. *Nat. Commun.* **9**:5422 (2018).
83. Yan, C. et al. Coordinatively unsaturated nickel–nitrogen sites towards selective and high-rate CO_2 electroreduction. *Energy Environ. Sci.* **11**, 1204-1210 (2018).
84. Fu, X. et al. Tailoring FeN_4 sites with edge enrichment for boosted oxygen reduction performance in proton exchange membrane fuel cell. *Adv. Energy Mater.* **9**, 1803737 (2019).
85. Jiang, R. et al. Edge-site engineering of atomically dispersed Fe–N_4 by selective C–N bond cleavage for enhanced oxygen reduction reaction activities. *J. Am. Chem. Soc.* **140**, 11594-11598 (2018).

86. Rong, X., Wang, H. J., Lu, X. L., Si, R. & Lu, T. B. Controlled synthesis of a vacancy-defect single-atom catalyst for boosting CO_2 electroreduction. *Angew. Chem. Int. Ed.* **59**, 1961-1965 (2020).
87. Qu, Y. et al. Thermal emitting strategy to synthesize atomically dispersed Pt metal sites from bulk Pt metal. *J. Am. Chem. Soc.* **141**, 4505-4509 (2019).
88. Zhang, L. et al. Coordination of atomic Co–Pt coupling species at carbon defects as active sites for oxygen reduction reaction. *J. Am. Chem. Soc.* **140**, 10757-10763 (2019).
89. Zeng, X. et al. Single-atom to single-atom grafting of Pt_1 onto Fe-N_4 center: Pt_1@Fe-N-C multifunctional electrocatalyst with significantly enhanced properties. *Adv. Energy Mater.* **8**, 1701345 (2017).
90. Jiao, J. et al. Copper atom-pair catalyst anchored on alloy nanowires for selective and efficient electrochemical reduction of CO_2. *Nat. Chem.* **11**, 222-228 (2019).
91. Bai, L., Hsu, C. S., Alexander, D. T., Chen, H. M. & Hu, X. A cobalt–iron double-atom catalyst for the oxygen evolution reaction. *J. Am. Chem. Soc.* **141**, 14190-14199 (2019).
92. Liu, L. et al. Determination of the evolution of heterogeneous single metal atoms and nanoclusters under reaction conditions: which are the working catalytic sites? *ACS Catal.* **9**, 10626-10639 (2019).
93. Wang, H. et al. Surpassing the single-atom catalytic activity limit through paired Pt-O-Pt ensemble built from isolated Pt_1 atoms. *Nat. Commun.* **10**:3808 (2019).
94. Kaiser, S. K. et al. Nanostructuring unlocks high performance of platinum single-atom catalysts for stable vinyl chloride production. *Nat. Catal.* **3**, 376-385 (2020).
95. Kleis, J. et al. Finite size effects in chemical bonding: from small clusters to solids. *Catal. Lett.* **141**, 1067-1071 (2011).
96. Li, L. et al. Investigation of catalytic finite-size-effects of platinum metal clusters. *J. Phys. Chem. Lett.* **4**, 222-226 (2013).
97. Eberhardt, W. et al. Photoemission from mass-selected monodispersed Pt clusters. *Phys. Rev. Lett.* **64**, 780 (1990).
98. Kaden, W. E., Wu, T., Kunkel, W. A. & Anderson, S. L. Electronic structure controls reactivity of size-selected Pd clusters adsorbed on TiO_2 surfaces. *Science* **326**, 826-829 (2009).
99. Roberts, F. S., Kane, M. D., Baxter, E. T. & Anderson, S. L. Oxygen activation and CO oxidation over size-selected Pt_n/alumina/Re(0001) model catalysts: correlations with valence electronic structure, physical structure, and binding sites. *Phys. Chem. Chem. Phys.* **16**, 26443-26457 (2014).

100. Roberts, F. S., Anderson, S. L., Reber, A. C. & Khanna, S. N. Initial and final state effects in the ultraviolet and X-ray photoelectron spectroscopy (UPS and XPS) of size-selected Pd_n clusters supported on TiO_2(110). *J. Phys. Chem. C* **119**, 6033-6046 (2015).
101. Greiner, M. T. et al. Free-atom-like *d* states in single-atom alloy catalysts. *Nat. Chem.* **10**, 1008-1015 (2018).
102. Thirumalai, H. & Kitchin, J. R. Investigating the reactivity of single atom alloys using density functional theory. *Top. Catal.* **61**, 462-474 (2018).
103. Dai, Y. et al. Inherent size effects on XANES of nanometer metal clusters: size-selected platinum clusters on silica. *J. Phys. Chem. C* **121**, 361-374 (2017).
104. Zandkarimi, B. et al. Interpreting the operando XANES of surface-supported subnanometer clusters: when fluxionality, oxidation state, and size effect fight. *J. Phys. Chem. C* **124**, 10057-10066 (2020).
105. Ramasse, Q. M. et al. Probing the bonding and electronic structure of single atom dopants in graphene with electron energy loss spectroscopy. *Nano Lett.* **13**, 4989-4995 (2013).
106. Nicholls, R. J. et al. Probing the bonding in nitrogen-doped graphene using electron energy loss spectroscopy. *ACS Nano* **7**, 7145-7150 (2013).
107. Kepaptsoglou, D. et al. Electronic structure modification of ion implanted graphene: the spectroscopic signatures of *p*-and *n*-type doping. *ACS Nano* **9**, 11398-11407 (2015).
108. Susi, T. et al. Single-atom spectroscopy of phosphorus dopants implanted into graphene. *2D Mater.* **4**, p.021013 (2017).
109. Gao, W. et al. Real-space charge-density imaging with sub-ångström resolution by four-dimensional electron microscopy. *Nature* **575**, 480-484 (2019).
110. Ishikawa, R. et al. Direct electric field imaging of graphene defects. *Nat. Commun.* **9**:3878 (2018).
111. Shibata, N. et al. Direct visualization of local electromagnetic field structures by scanning transmission electron microscopy. *Acc. Chem. Res.* **50**, 1502-1512 (2017).
112. Shibata, N. et al. Electric field imaging of single atoms. *Nat. Commun*. **8**:15631 (2017).
113. Tierney, H. L., Baber, A. E. & Sykes, E. C. H. Atomic-scale imaging and electronic structure determination of catalytic sites on Pd/Cu near surface alloys. *J. Phys. Chem. C* **113**, 7246-7250 (2009).
114. Sobotík, P. et al. Emergence of state at Fermi level due to the formation of In-Sn heterodimers on Si(100)-2×1. *Phy. Rev. B* **88**, 205406 (2013).

115. Zhu, Y. et al. Modulating the electronic structure of single-atom catalysts on 2D nanomaterials for enhanced electrocatalytic performance. *Small Methods* **3**, 1800438 (2019).
116. Hossain, M. D. et al. Rational design of graphene-supported single atom catalysts for hydrogen evolution reaction. *Adv. Energy Mater.* **9**, 1803689 (2019).
117. Back, S., Lim, J., Kim, N. Y., Kim, Y. H. & Jung, Y. Single-atom catalysts for CO_2 electroreduction with significant activity and selectivity improvements. *Chem. Sci.* **8**, 1090-1096 (2017).
118. Cao, R. et al. Promotion of oxygen reduction by a bio-inspired tethered iron phthalocyanine carbon nanotube-based catalyst. *Nat. Commun.* **4**:2076 (2013).
119. Lai, Q. Metal–organic-framework-derived Fe-N/C electrocatalyst with five-coordinated Fe-N_x sites for advanced oxygen reduction in acid media. *ACS Catal.* **7**, 1655-1663 (2017).
120. Yin, P. et al. Single cobalt atoms with precise N-coordination as superior oxygen reduction reaction catalysts. *Angew. Chem. Int. Ed.* **55**, 10800-10805 (2016).
121. Han, J. et al. Reordering *d* orbital energies of single-site catalysts for CO_2 electroreduction. *Angew. Chem. Int. Ed.* **58**, 12711-12716 (2019).
122. Deng, J. et al. Multiscale structural and electronic control of molybdenum disulfide foam for highly efficient hydrogen production. *Nat. Commun.* **8**: 14430 (2017).
123. Deng, J. et al. Triggering the electrocatalytic hydrogen evolution activity of the inert two-dimensional MoS_2 surface via single-atom metal doping. *Energy Environ. Sci.* **8**, 1594-1601 (2015).
124. Luo, Z. et al. Chemically activating MoS_2 via spontaneous atomic palladium interfacial doping towards efficient hydrogen evolution. *Nat. Commun.* **9**: 2120 (2018).
125. Zhang, J., Xu, X., Yang, L., Cheng, D. & Cao, D. Single-atom Ru doping induced phase transition of MoS_2 and S vacancy for hydrogen evolution reaction. *Small Methods* **3**, 1900653 (2019).
126. Guan, E. et al. Supported metal pair-site catalysts. *ACS Catal.* **10**, 9065-9085 (2020).
127. Jiang, J., Ding, W., Li, W. & Wei, Z. Freestanding single-atom-layer Pd-based catalysts: oriented splitting of energy bands for unique stability and activity. *Chem* **6**, 431-447 (2020).
128. Kip, B. J., Duivenvoorden, F. B. M., Koningsberger, D. C. & Prins, R. Determination of metal particle size of highly dispersed Rh, Ir, and Pt catalysts by hydrogen chemisorption and EXAFS. *J. Catal.* **105**, 26-38 (1987).

129. Kruppe, C. M., Krooswyk, J. D. & Trenary, M. Polarization-dependent infrared spectroscopy of adsorbed carbon monoxide to probe the surface of a Pd/Cu(111) single-atom alloy. *J. Phys. Chem. C* **121**, 9361-9369 (2017).
130. Matsubu, J. C., Yang, V. N. & Christopher, P. Isolated metal active site concentration and stability control catalytic CO_2 reduction selectivity. *J. Am. Chem. Soc.* **137**, 3076-3084 (2015).
131. Yubing, L. et al. A versatile approach for quantification of surface site fractions using reaction kinetics: The case of CO oxidation on supported Ir single atoms and nanoparticles. *J. Catal.* **378**, 121-130 (2019).
132. Resasco, J. et al. Relationship between atomic scale structure and reactivity of Pt catalysts: hydrodeoxygenation of *m*-cresol over isolated Pt cations and clusters. *ACS Catal.* **10**, 595-603 (2019).
133. Millet, M. M. Ni single atom catalysts for CO_2 activation. *J. Am. Chem. Soc.* **141**, 2451-2461 (2019).
134. Lang, R. et al. Non defect-stabilized thermally stable single-atom catalyst. *Nat. Commun.* **10**:234 (2019).
135. Nesselberger, M. et al. The effect of particle proximity on the oxygen reduction rate of size-selected platinum clusters. *Nat. Mater.* **12**, 919-924 (2013).
136. Chen, Z. W., Chen, L. X., Yang, C. C. & Jiang, Q. Atomic (single, double, and triple atoms) catalysis: frontiers, opportunities, and challenges. *J. Mater. Chem. A* **7**, 3492-3515 (2019).
137. Zhang, J. et al. Supported dual-atom catalysts: preparation, characterization, and potential applications. *Chin. J. Catal.* **41**, 783-798 (2020).
138. Goodman, E. D. et al. Catalyst deactivation via decomposition into single atoms and the role of metal loading. *Nat. Catal.* **2**, 748-755 (2019).
139. Prieto, G., Zečević, J., Friedrich, H., De Jong, K. P. & De Jongh, P. E. Towards stable catalysts by controlling collective properties of supported metal nanoparticles. *Nat. Mater.* **12**, 34-39 (2013).
140. Li, H. et al. Synergetic interaction between neighbouring platinum monomers in CO_2 hydrogenation. *Nat. Nanotechnol.* **13**, 411-417 (2018).
141. Mitchell, S. et al. Structural analysis of hierarchically organized zeolites. *Nat. Commun.* **6**: 8633 (2015).
142. Liu, J. C., Tang, Y., Wang, Y. G., Zhang, T. & Li, J. Theoretical understanding of the stability of single-atom catalysts. *Natl. Sci. Rev.* **5**, 638-641 (2018).

143. Jones, J. et al. Thermally stable single-atom platinum-on-ceria catalysts via atom trapping. *Science* **353**, 150-154 (2016).
144. Zhang, Z. et al. Thermally stable single atom Pt/*m*-Al_2O_3 for selective hydrogenation and CO oxidation. *Nat. Commun.* **8**:16100 (2017).
145. Nie, L. et al. Activation of surface lattice oxygen in single-atom Pt/CeO_2 for low-temperature CO oxidation. *Science* **358**, 1419-1423 (2017).
146. Li, X., Yang, X., Zhang, J., Huang, Y. & Liu, B. In situ/operando techniques for characterization of single-atom catalysts. *ACS Catal.* **9**, 2521-2531 (2019).
147. DeRita, L. et al. Structural evolution of atomically dispersed Pt catalysts dictates reactivity. *Nat. Mater.* **18**, 746-751 (2019).
148. Vorobyeva, E. et al. Activation of copper species on carbon nitride for enhanced activity in the arylation of amines. *ACS Catal.* **10**, 11069-11080 (2020).
149. Chen, Z. et al. A heterogeneous single-atom palladium catalyst surpassing homogeneous systems for Suzuki coupling. *Nat. Nanotechnol.* **13**, 702-707 (2018).
150. Tang, Y. et al. Rh single atoms on TiO_2 dynamically respond to reaction conditions by adapting their site. *Nat. Commun.* **10**: 4488 (2019).
151. Cao, L. et al. Identification of single-atom active sites in carbon-based cobalt catalysts during electrocatalytic hydrogen evolution. *Nat. Catal.* **2**, 134-141 (2019).
152. Cao, L. et al. Dynamic oxygen adsorption on single-atomic Ruthenium catalyst with high performance for acidic oxygen evolution reaction. *Nat. Commun.* **10**:4849 (2019).
153. Hansen, T. W., DeLaRiva, A. T., Challa, S. R. & Datye, A. K. Sintering of catalytic nanoparticles: particle migration or Ostwald ripening? *Acc. Chem. Res.* **46**, 1720-1730 (2013).
154. Liu, L. & Corma, A. Evolution of isolated atoms and clusters in catalysis. *Trends Chem.* **2**, 383-400 (2020).
155. Dessal, C. et al. Dynamics of single Pt atoms on alumina during CO oxidation monitored by operando X-ray and infrared spectroscopies. *ACS Catal.* **9**, 5752-5759 (2019).
156. Kaiser, S. K., Lin, R., Krumeich, F., Safonova, O. V. & Pérez-Ramírez, J. Preserved in a shell: high-performance graphene-confined ruthenium nanoparticles in acetylene hydrochlorination. *Angew. Chem. Int. Ed.* **58**, 12297-12304 (2019).
157. Liu, L. et al. Evolution and stabilization of subnanometric metal species in confined space by in situ TEM. *Nat. Commun.* **9**:574 (2018).

158. Paolucci, C. et al. Dynamic multinuclear sites formed by mobilized copper ions in NO_x selective catalytic reduction. *Science* **357**, 898-903 (2017).
159. Wang, Y.-G., Mei, D., Glezakou, V. A., Li, J. & Rousseau, R. Dynamic formation of single-atom catalytic active sites on ceria-supported gold nanoparticles. *Nat. Commun.* **6**:6511 (2015).
160. Bliem, R. et al. Dual role of CO in the stability of subnano Pt clusters at the Fe_3O_4 (001) surface. *Proc. Nat. Acad. Sci.* **113**, 8921-8926 (2016).
161. Sun, J. J. & Cheng, J. Solid-to-liquid phase transitions of sub-nanometer clusters enhance chemical transformation. *Nat. Commun.* **10**:5400 (2019).
162. Zafeiratos, S., Piccinin, S. & Teschner, D. Alloys in catalysis: phase separation and surface segregation phenomena in response to the reactive environment. *Catal. Sci. Technol.* **2**, 1787-1801.
163. Darby, M. T., Sykes, E. C. H., Michaelides, A. & Stamatakis, M. Carbon monoxide poisoning resistance and structural stability of single atom alloys. *Topics Catal.* **61**, 428-438 (2018)
164. Kaiser, S. K., Clark, A. H., Cartocci, L., Krumeich, F. & Pérez-Ramírez, J. Sustainable synthesis of bimetallic single atom gold-based catalysts with enhanced durability in acetylene hydrochlorination. *Small* doi:10.1002/smll.202004599 (2020).
165. Zhou, X. et al. Unraveling charge state of supported Au single-atoms during CO oxidation. *J. Am. Chem. Soc.***140**, 554-557 (2018).
166. Daelman, N., Capdevila-Cortada, M. & López, N. Dynamic charge and oxidation state of Pt/CeO_2 single-atom catalysts. *Nat. Mater.* **18**, 1215-1221 (2019).
167. Li, Y. et al. Complex structural dynamics of nanocatalysts revealed in Operando conditions by correlated imaging and spectroscopy probes. *Nat. Commun.* **6**:7583 (2015).
168. Zhao, J. Direct in situ observations of single Fe atom catalytic processes and anomalous diffusion at graphene edges. *Proc. Nat. Acad. Sci.* **111**, 15641-15646 (2014).
169. Resasco, J. & Christopher, P. Atomically dispersed Pt-group catalysts: reactivity, uniformity, structural evolution, and paths to increased functionality. *J. Phys. Chem. Lett.* **11**, 10114-10123 (2020).
170. Chen, Y., Sun, H. & Gates, B. C. Prototype atomically dispersed supported metal catalysts: iridium and platinum. *Small* doi.org/10.1002/smll.202004665 (2020).

Acknowledgement

This publication was created as part of NCCR Catalysis, a National Centre of Competence in Research funded by the Swiss National Science Foundation.

Author contributions

S.M. and J.P.-R. conceived and wrote this review together.

Competing interests

The authors declare no competing interests.

Figures

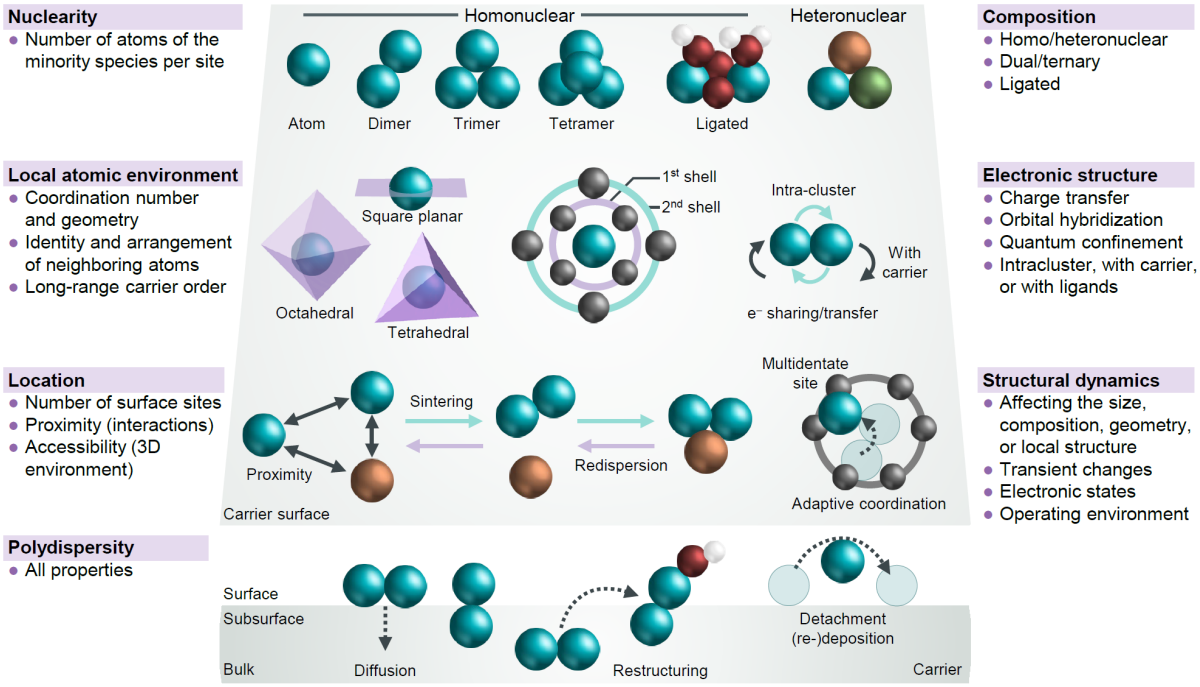

Fig. 1 | Structural characteristics of supported low-nuclearity catalysts. Top (upper panel) and side (lower panel) views of metal atoms and clusters (blue, orange, and green spheres) supported on suitable carriers (grey shaded areas) illustrating the multiple properties that can influence their reactivity. Besides the number and composition of metal atoms in the low-nuclearity species, it is also crucial to know their local atomic environment, whether ligands are present, the location, and structural dynamics, which all impact the electronic structure. Non-uniformity in any of these properties can result in a high polydispersity calling for a statistical representation of distinct ensembles in the catalyst.

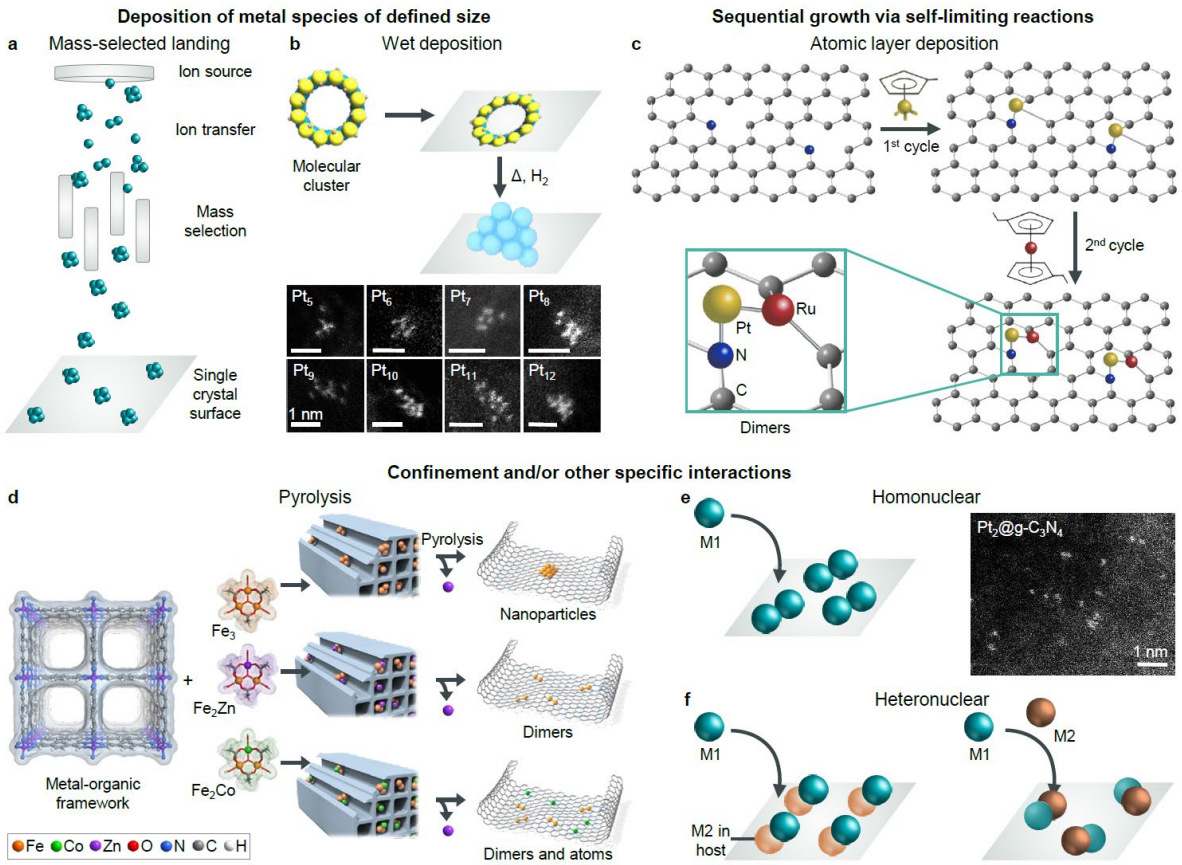

Fig. 2 | Approaches to stabilize metal species with precise numbers of atoms on suitable carriers. **a**,**b |** The deposition of metal precursors of pre-defined size is among the most versatile strategies for controlling nuclearity. Typical methods to achieve this include the mass-selected landing of ionic species on single-crystal surfaces (panel **a**) and the wet deposition of molecular clusters on various carriers followed by their thermal decomposition to remove associated ligands (panel **b**), as illustrated for Pt tiara complexes ranging from 5-12 metal atoms. **c-f |** Other approaches are known to yield specific nuclearities and compositions. For example, the sequential growth via self-limiting reaction, performed by atomic-layer deposition (panel **c**), can access homo- or heteronuclear dimers, as exemplified for Pt-Ru supported on nitrogen-doped carbons. Pyrolysis routes typically exploit strong interactions and confinement of precursors deposited on porous materials such as MOFs (panel **d**). Preferential interactions between different metals can influence the resulting speciation. In some systems, energetic factors may lead to the favourable stabilization of low-nuclearity species of defined size. For example, Pt dimers were visible after the wet deposition of Pt nitrate on graphitic carbon nitride (AC-STEM image, panel **e**) and corresponded to be the most stable species evidenced by DFT. Similarly, reported strategies to form heteronuclear dimers include exploiting the affinity between metal atoms in solution with other metals in the carrier or solution (panel **f**). Panels b and c adapted with permission from refs. 19 and 30, Springer Nature. Panel d adapted with permission from ref. 32, Wiley Verlag.

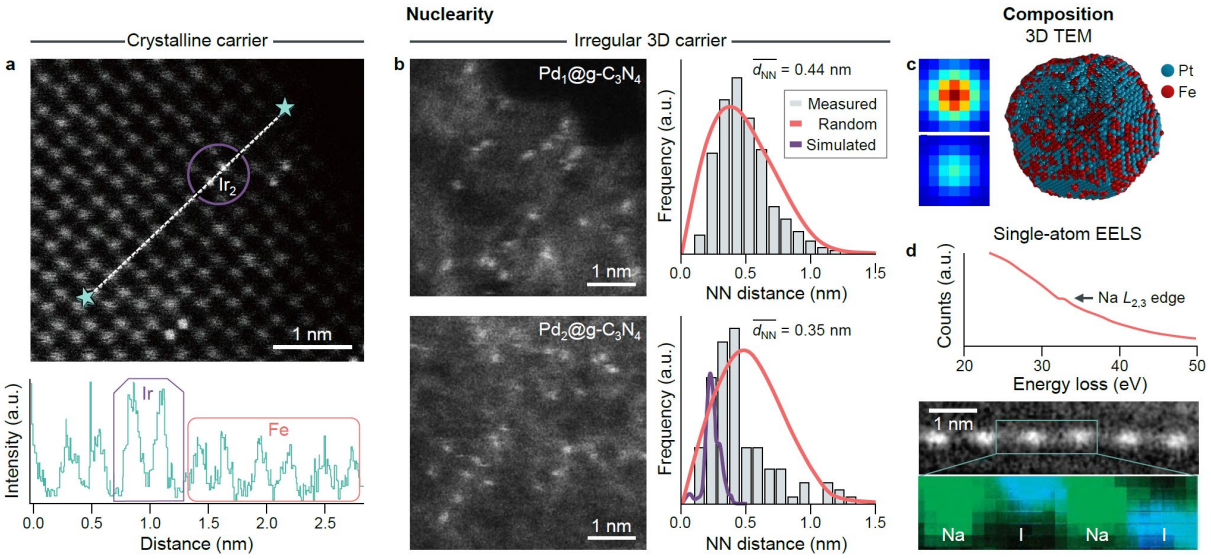

Fig. 3 | Determination of nuclearity and composition. **a |** Direct visualization of Ir dimers by AC-STEM. The intensity profile along the dashed line in the micrograph is plotted below. **b |** AC-STEM images of Pd atoms and dimers on graphitic carbon nitride. The graphs show the frequency of measured nearest-neighbour distances (d_{NN}) between atoms compared to the distributions theoretically expected for a random distribution and computed by molecular dynamics simulations (for dimers). **c |** Three-dimensional reconstruction of the positions of Fe (red) and Pt (blue) atoms in a nanoparticle derived by a multi-slice STEM imaging method using local intensity distributions (shown left). **d |** Single-atom electron energy loss spectroscopy of light elements. The graph displays the electron energy loss spectrum of the one-dimensional sodium iodide atomic chain observed in the STEM image (top panel) and the derived elemental map (bottom panel). The inset shows the atomic structure. Panel **a** adapted with permission from ref. 21, National Academy of Sciences. Panels **c** and **d** adapted with permission from refs. 49 and 52, Springer Nature.

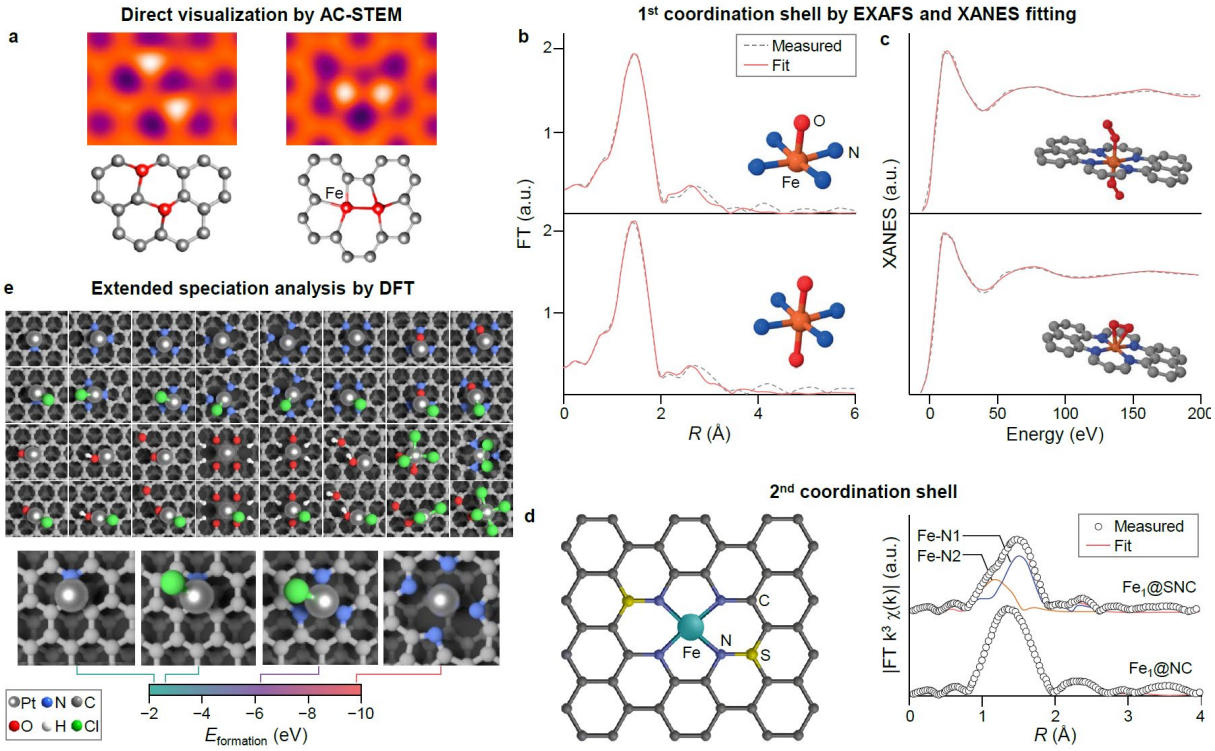

Fig. 4 | Discrimination of the local-atomic structure. **a |** AC-STEM images of Fe dimers in distinct types of vacancies in graphene and corresponding atomic structures; quadvacancy (left) and two adjacent monovacancies (right). **b,c |** Determination of the first coordination shell of Fe single atoms in nitrogen-doped carbons. Fits in the Fourier transformed space of the Fe K-edge EXAFS spectra showing that either a square-pyramidal or a distorted octahedral coordination can reproduce the measured data with the same accuracy (panel **b**). Fitting of the K-edge XANES data overlaying the theoretical spectrum for the two depicted structures (panel **c**), both incorporating a dioxygen molecule, able to reproduce the experimental spectrum. **d |** Modification of the second coordination shell. Proposed structure of Fe atoms stabilized on S,N-doped graphene (SNC) and quantitative EXAFS fits identifying two distinct Fe-N_x contributions in Fe@SNC compared to Fe@NC. **e |** Extended matrix generated to screen the potential atomic structures of Pt atoms stabilized on heteroatom-doped carbons by DFT (top), and a subset of structures emphasizing the large variation in the energy of formation, illustrated for nitrogen-based coordination sites in the presence or absence of Cl ligands. Panel **a** adapted with permission from ref. 73, ACS Publications. Panels **b**,**c** adapted with permission from ref. 77, Springer Nature. Panel **d** adapted from ref. 81 with permission of Wiley-VCH.

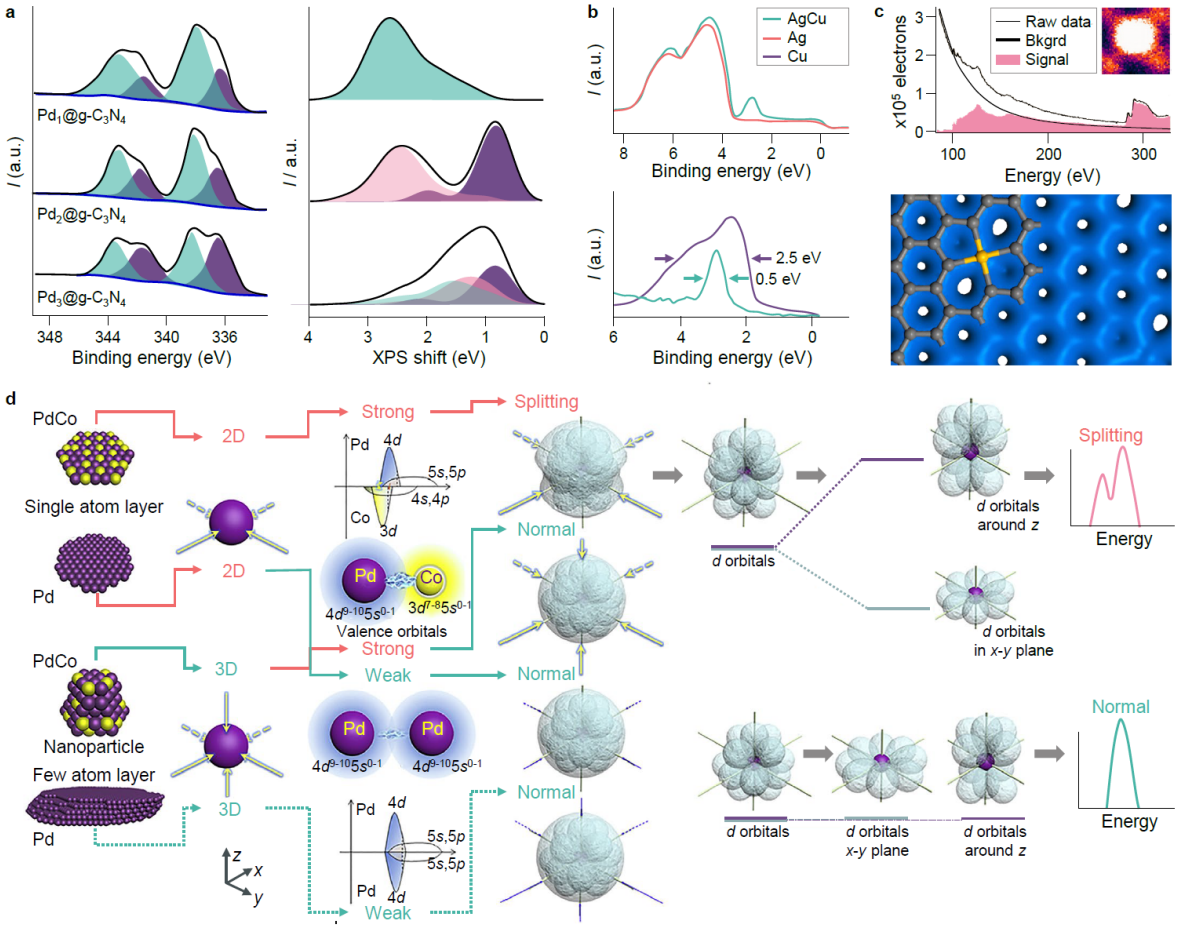

Fig. 5 | Electronic properties of low-nuclearity metal species. **a |** Measured (left) and simulated (right) Pd 3*d* core-level XPS spectra of Pd atoms, dimers, and trimers on graphitic carbon nitride. In measured spectra, black lines show the fitted results, shaded areas the deconvoluted components indicating tentative assignments, and blue lines the background. In theoretical spectra, shaded areas represent each atom in the ensemble. **b |** The measured valence photoemission spectra of a Cu-Ag single-atom alloy (top graph) reveal the narrow Cu 3*d* states at a binding energy of ~2.5 eV. The difference spectrum of AgCu and Ag plotted with a Cu reference spectrum (bottom), show that the Cu 3*d* states are one-fifth the width they are in bulk Cu. **c |** A combination of AC-STEM, EELS, and calculations reveal striking electronic difference between two distinct single substitutional Si defect geometries in graphene. High-resolution EELS spectrum (top) of a Si atom in 4-fold coordination (image inset) and simulated orbital isosurface (bottom) in which orbitals are visibly bridging across intrinsic holes in the graphene lattice, evidencing *d*-band hybridization. **d |** Strategy to induce orbital splitting by developing 2D-oriented coordination of cobalt and palladium in single-atom layers. Panel b adapted with permission from ref. 101, Springer Nature. Panel c adapted with permission from ref. 105, ACS Publications. Panel d adapted with permission from ref. 127, Cell Press.

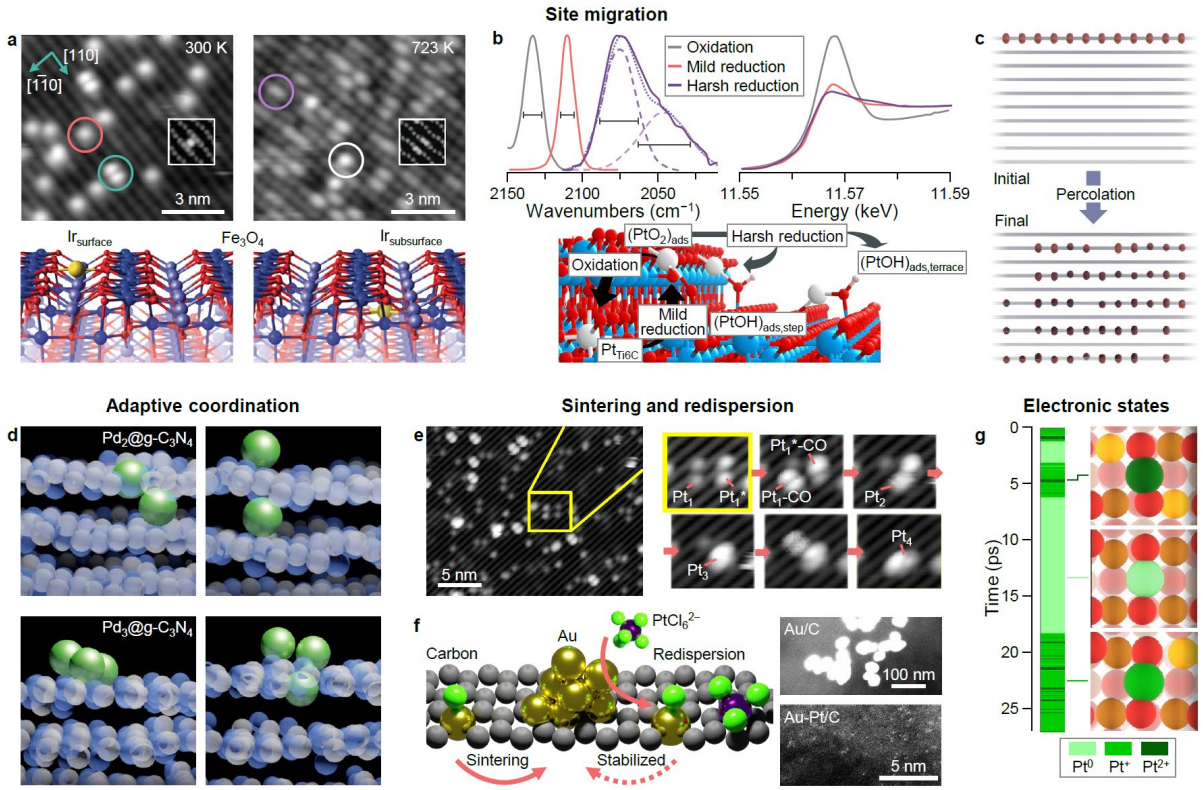

Fig. 6 | Types of structural dynamics of low-nuclearity species. **a |** STM images and calculated structures or Ir species on Fe_3O_4. Ir adatoms (red circle) and dimers (blue circle) are visible in the as-deposited material, while upon heating iridium centers migrate and substitute Fe centres in surface (grey circle) and subsurface (purple circle) positions. **b |** Infrared spectra of adsorbed CO (top left) and XANES spectra (top right) evidencing distinct characteristics of Pt single atoms on TiO_2 following various oxidative or reductive pre-treatments (dashed lines). Schematic showing the proposed dynamic evolution. **c |** Initial and final states of kMC simulations predicting the percolation of copper atoms, initially deposited on the surface, into the bulk of a graphitic carbon nitride host. **d |** Snapshots of molecular dynamics simulations of Pd dimers, and trimers stabilized on graphitic carbon nitride illustrating distinct possible configurations. **e |** STM image sequence following the CO-induced diffusion and coalescence of Pt adatoms on $Fe_3O_4(001)$. **f |** Scheme showing the typical sintering path of Au single atoms on carbon carriers upon heating. The resulting Au nanoparticles can be redispersed by introducing $PtCl_6^{2-}$ forming bimetallic single-atom catalysts with improved sintering resistance. AC-STEM images of the Au/C and Au-Pt/C catalysts after thermal treatment at 873 K. **g |** Structure of Pt atoms coordinated to two O atoms on the $CeO_2(100)$ surface (top) and time evolution of the atom-resolve oxidation states of the Pt and surface Ce atoms. Panel a adapted with permission from ref. 66, Wiley Verlag. Panels b and g adapted with permission from refs. 147 and 166, Springer Nature. Panel e adapted with permission from ref. 160, National Academy of Sciences.